1993

The topological structure of the steady, laminar three-vortex system for a cylinder-flat plate juncture : an experimental investigation

John P. Fitzgerald
Lehigh University

AUTHOR:

Fitzgerald, John P.

TITLE:

The Topological Structure of the Steady, Laminar Three-Vortex System for a Cylinder-Flat Plate Juncture: An Experimental Investigation

DATE: October 10, 1993

Lehigh University

The Topological Structure of the Steady, Laminar Three-Vortex System for a Cylinder-Flat Plate Juncture: An Experimental Investigation

John P. Fitzgerald

A Thesis

Presented to the Graduate Committee

of Lehigh University

in Candidacy for the Degree of

Master of Science

in

Mechanical Engineering

August 1993

Department of Mechanical Engineering & Mechanics
Lehigh University, Bethlehem, PA 18015

Certificate of Approval

This thesis is accepted and approved in partial fulfillment of the requirements for the degree of Master of Science.

Date: August 4, 1993

Professor in Charge
Dr. Charles R. Smith

Department Chairperson
Dr. Robert P. Wei

DEDICATION

To My Loving Parents

Thomas and Frances

ACKNOWLEDGMENTS

Thanks to my advisor Dr. Chuck Smith for his technical guidance and extreme patience above and beyond the call of duty in overseeing this research and especially for making experimental fluid mechanics fun.

Also thanks to my fellow "Smith" coworkers in the lab, for their help and friendship, - Chuck, Jin and Levent. Additionally, I would like to thank all the people who directly made this research "physically" possible, - Dick, Jimmy, and Bob in the machine shop.

Additional thanks to Dr. D. Rockwell for use of his laser scanning equipment in this research effort and all the others in the lab, too many to enumerate, you all know who you are. Thank you for your friendship and assistance. Also, to Özgür Akin, one of the best human beings that I had the good fortune to meet, your close friendship and technical guidance through my trials and tribulations at Lehigh will never be forgotten.

A special thanks to Kelly for her never-ending love and understanding in helping me reach my goals.

With warmest love and gratitude to my parents, to whom that this thesis is dedicated. Without your infinite love, assistance and life-guidance, I would have never pursued the impossible.

The continuing support of the Air Force Office of Scientific Research under grant AFSOR-91-0218 is also greatly appreciated.

TABLE OF CONTENTS

LIST OF FIGURES

NOMENCLATURE

D, h	cylinder diameter and height
δ^*	displacement thickness
δ_o	boundary layer thickness
β_P	separation parameter
u_∞	free stream velocity
u'/u_∞	turbulence intensity
ν	kinematic viscosity
Re_D	Reynolds number based on cylinder diameter
Re_{δ^*}	Reynolds number based on displacement thickness
Re_x	Reynolds number based on x (front edge of cylinder location)
N, N′	nodes and hlaf-nodes respecitively
S, S′	saddle and half-saddle points respectively
x, y, z	Cartesian coordinates (origin at the leading edge)
$\omega_x, \omega_y, \omega_z$	vorticity components in x, y and z directions
η_x	$\partial\omega_y/\partial x$
ξ_y	$\partial\omega_x/\partial y$

Subscripts

A, S	denote attachment and separation respectively
1 2 3...	numbering order of primary and secondary vortices

ABSTRACT

The topological structure of the steady, laminar three-vortex system formed at a cylinder-flat plate juncture has been studied experimentally employing hydrogen bubble flow visualization in a low-speed recirculating water channel. A new type of steady, laminar three-vortex system is identified, which supports recent computational studies. The flat plate skin-friction patterns corresponding to both the new and to the standard three-vortex topology are found to be equivalent, indicating the non-unique relationship between the wall-limiting streamline pattern and the three-dimensional flow above the plate. For the new topology, the foremost line of coalescence is a line of attachment rather than a line of separation. This unusual feature illustrates that convergence of skin-friction lines is a necessary, but not sufficient condition indicative of a line of separation.

At least three different types of steady, laminar, three-vortex topologies are shown to exist; these are compared and contrasted with previous experimental and computational studies. A unique relationship between the three-vortex topologies has been successfully established based on non-dimensional parameters employing cylinder geometry and boundary layer properties.

1.0 INTRODUCTION

1.1 General

It is commonly understood that for certain ranges of Reynolds number, the boundary layer flow along a flat-plate surface will separate and roll up to form a steady, laminar three-vortex system when encountering a bluff body obstruction (such as a cylinder or a wing). This steady, separated vortical flow within the cylinder/flat-plate juncture is highly three-dimensional and subject to extreme changes in overall topological structure for small changes in the non-dimensional boundary layer parameter D/δ^*. The sensitivity of these lower Reynolds number flows suggests the need for further examination of this basic flow behavior, with a view toward providing basic understanding applicable to the behavior of higher speed flows and more complex geometries.

The balance of this introduction reviews previous relevant research, followed by a definition of the objectives of the present study.

1.2 Related Works

1.2.1 General Steady Laminar Juncture Flow

Several previous experimental, numerical and theoretical studies have attempted to document the characteristics of steady, laminar juncture flows. Experimental techniques employed include smoke or hydrogen bubble flow visualization, surface visualization using oil suspensions, and laser-particle methods such as particle image velocimetry. Theoretical studies have employed critical point concepts to account for the general topological structure of steady, laminar juncture flows. These critical point concepts, coupled with extensive numerical studies, can aid the experimentalist in searching for

and identifying various types of flow structures. While many details of steady, laminar juncture flow have been documented, no study to date has successfully paramerterized the flow conditions leading to the appearance of the different vortex topologies that can occur when a steady, laminar three-vortex system (shown schematically in Figure 1.1) is present.

In a wind tunnel study of steady, laminar juncture flow, Norman (1972) employed smoke visualization to examine the flow patterns for a series of square bodies of varying widths and heights mounted on a flat plate. Norman visualized the flow using both a smoke sheet, generated by galvanic heating of a 13 cm long nichrome ribbon (0.3 mm thick by 1.5 mm wide) coated with paraffin wax, and smoke injected through holes in the endwall. From his observations of a broad range of steady, laminar juncture flows, Norman established the existence of two distinct, three-vortex topologies: the standard Jet-Maze topology and the Stairstep topology, represented in 2-D streamline schematics in Figure 1.2 . In the Jet-Maze topology (Figure 1.2a), the flow in the upper portion of the boundary layer, where stagnation pressures are highest, navigates around vortex 1, reverses direction at the obstacle base, and travels upstream like a jet through an intricate path to additionally feed vortices 2 and 3. Hence the name: Jet-Maze. However, in the Stairstep topology (Figure 1.2b), each vortex is fed individually from upstream by singular shear layers of fluid in a step-wise fashion. Hence the name: Stairstep. Even though Norman established the presence of the Stairstep topology, he could determine no clear steady case. In a similar study, Sedney and Kitchens (1975), employing a vapor-screen technique, a method in which one observes the light scattered by liquid or solid water particles introduced into the flow, observed streamline dynamics similar to Norman (Figure 1.2) for various bluff bodies, but chose to characterize it as a Jet-Maze topology over a Stairstep topology.

The laminar horseshoe vortex system formed around the base of cylinders of varying heights mounted normal to a flat plate was investigated by Baker (1979). Employing smoke generation techniques similar to Norman, Baker systematically located a smoke filament at different heights above the surface, allowing him to explore the 'feeding layers'* of the steady, laminar three-vortex system. Baker proposed the existence of a single steady, laminar three-vortex topology which was different from either of Norman's two topologies. Figure 1.3a shows Baker's hypothesized streamline schematic, including the location of all separation and attachment points associated with the steady, laminar three-vortex topology. In Baker's topology, vortex 3 is fed twice, similar to the Jet-Maze topology, yet his topology suggests step-wise feeding of the remaining vortices, which is characteristic of the Stairstep topology. Due to photographic difficulties, Baker's topology is partially conjectured since he could not clearly establish which of vortices 2 or 3 was fed first as the smoke filament was brought closer to the plate. Using this smoke filament visualization, Baker determined the parameter space over which the steady laminar three vortex system exists. Figure 1.3b shows the boundaries of this parameter space based on the dimensionless parameters D/δ^* and Re_D.

In a study of the many characteristics of laminar juncture flows, Perry and Fairlie (1974) based on 'phase-space' and 'phase-plane' methods that utilize critical-point concepts, established three basic types of flow separation. Critical points are points in a flow field where the streamline slope is indeterminate and the velocity is zero relative to an appropriate reference point such as a separation, attachment or saddle point. In Figure 1.3a, Baker's topology, the critical points are indicated by SP1, SP2, A1, S1, etc. Asymptotically-correct, first-ordered solutions of the Navier-Stokes and continuity

* A feeding layer is a shear layer within the hydrodynamic boundary layer.

equations can be derived close to the critical points, which allow much of the remaining flow topology to be deduced, since there are only a limited number of ways that the streamlines can be joined. Perry and Fairlie showed, for certain parameters, that there are three types of symmetric three-dimensional laminar separation. Here, the term 'separation' is ambiguous since, as Figures 1.4 and 1.5 indicate, there can also be a point of attachment. The type of critical point is characterized by the parameter η_x/ξ_y, where ξ and η are the vorticity components in the respective x and y directions, with the subscript indicating the derivative in the indicated direction. The value of parameter η_x/ξ_y dictates which of the three types of symmetric, three-dimensional laminar flow separation is present. As shown in Figures 1.4 and 1.5, if $\eta_x/\xi_y > 1$, the outermost singular point is a saddle point of separation, whereas $\eta_x/\xi_y < 1$ indicates a saddle point of attachment. Lastly, if $\eta_x/\xi_y = 1$, the outermost singular point is indeterminant, and can fluctuate between either a point of separation or attachment. Later, Perry and Chong (1987) improved upon the Perry and Fairlie technique and included higher-order terms to obtain asymptotically exact solutions of the Navier-Stokes and continuity equations close to the critical points, providing even greater insight into the details of the surrounding flow.

In an extension of the Perry and Fairlie technique, Hunt, et al. (1978) examined the kinematics of streamline patterns in laminar flows around three-dimensional surface obstacles, deriving certain topological constraints for the flow near the critical points. For two-dimensional plane sections of the flow, the critical points must satisfy the relation:

$$\left(\sum N+\frac{1}{2}\sum N'\right)-\left(\sum S+\frac{1}{2}\sum S'\right)=n-1 \qquad (1.1)$$

where n represents the connectivity of the flow region, ΣN denotes the sum of the nodes, ΣS is the sum of the saddles, and the primed sums indicate half-nodes and half-saddles. Figure 1.6 illustrates the classification of critical points based on a simple flow situation adapted from Hunt et al. Further details of (1.1) and its application to the three flow regimes established by the present study are discussed in detail in Chapter 4.

Hunt et al. showed by kinematic analysis that experimental shear-stress patterns can be distinguished as either separation or attachment points. To support their analytical work, they performed flow-visualization experiments in a wind tunnel employing an oil-film technique to obtain high-resolution, mean shear-stress lines near the singular points of various juncture flows; the oil-film employed a powder suspension in oil. After the wind tunnel had been run for a period of time, the flow moved the suspended particles into consistent patterns which reflected the skin-friction-patterns (lines of coalescence and divergence), or "footprints" of the flow. These "footprints," identified the separation or attachment lines/points and, when coupled with theory, allowed the general flow pattern to be effectively determined.

A computational study of the laminar horseshoe vortex system formed at a cylinder/plate juncture was performed by Visbal (1991). Using a fully-vectorized, time-accurate, three-dimensional Navier-Stokes solver that employs an implicit approximate-factorization Beam-Warming algorithm, Visbal computed the flow for two different incoming boundary layer characteristics. In some cases, an initial boundary layer of thickness $\delta_o/D = 0.1$ was assumed 20 diameters upstream $(x/D = -20)$ of the cylinder. For the remaining cases, the boundary layer was allowed to develop from the flat plate leading edge located at $x/D = -2.0$ Visbal's study revealed that for certain values of a separation parameter β_p, a previously undiscovered type of steady, laminar three-vortex topology would develop, for which the foremost line of coalescence is a line of

attachment rather than a line of *separation*. In his study, Visbal employed a separation parameter defined by

$$\beta_P = \left(\partial\omega_y/\partial x\right)\Big/\left(\partial\omega_x/\partial y\right), \tag{1.2}$$

where ω_y and ω_x are the vorticity components in the y and x directions, respectively. It is important to note that this parameter corresponds exactly with Perry and Fairlie's parameter, which governs which of the three types of separation conditions exist for a flow (Figures 1.4 & 1.5). Visbal determined that the outermost critical point is 1)a separation point (Jet-Maze topology) for $\beta_P > 1$ and 2) a point of attachment (Attachment topology) for $\beta_P < 1$ indicating consistency with the method of Perry and Fairlie (1974). Visbal's sketches of the two topologies are shown in Figure 1.7. Note that Visbal's Attachment topology (Figure 1.7b) indicates that the three vortices are fed in a step-wise fashion similar to that of the Stairstep topology proposed by Norman. Visbal computationally demonstrated the existence of both the topologies of Figure 1.7, examining a case with $\beta_P < 1$ ($Re_D = 2600$ with $\delta_o/D = 0.1$), and a case for $\beta_P > 1$ ($Re_D = 3500$ with the leading edge at $x/D = -2.0$).

In that same year, Hung et al. (1991), employing an explicit 3rd-order Runge-Kutta method to solve the time-dependent Navier-Stokes equations, published computational results similar to Visbal. In contrast to Visbal's study, in which he prescribed a constant impinging boundary layer thickness, Hung et al. initiated the inflow boundary layer 10 diameters in front of the cylinder and allowed a Blasius boundary layer to grow and develop according to the formula:

$$\delta = \frac{5.0x}{Re_x^{1/2}}$$

For a computational case corresponding to $M_\infty = 2.0$ and $Re_D = 1500$, a steady three-vortex topology with an outermost critical point of attachment developed, as shown in

Figure 1.8. Even though Hung et al. employed different numerical schemes and different incoming flow boundary conditions than Visbal, their results for similar ranges of Re_D agree closely with Visbal's, suggesting that the Attachment topology is not an anomaly of the solution technique.

1.3 Objectives

While many of the characteristics of laminar juncture flows have been explored and documented, no study has successfully explained the appearances of the several different three-vortex systems. Different researchers have also reported markedly different laminar, three-vortex topologies, leaving open the question of the correct topology and/or its variation with controlling parameters.

The objectives of the present study are as follows:

(i) To experimentally examine the cylinder/flat plate juncture region over a wide range of flow parameters and clearly establish the different characteristics of the steady, laminar three-vortex systems that form in the juncture region.

(ii) To compare and contrast the observed topological results of (i) with the results of previous studies;

(iii) To establish the influence of geometric and flow parameters (u_∞, D, δ^*, etc.) on the characteristics of the steady, laminar three-vortex system.

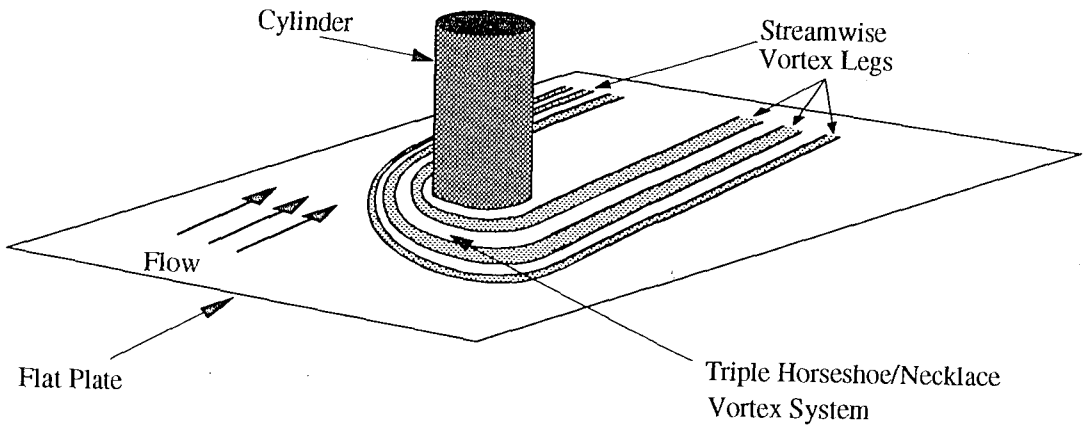

(a)

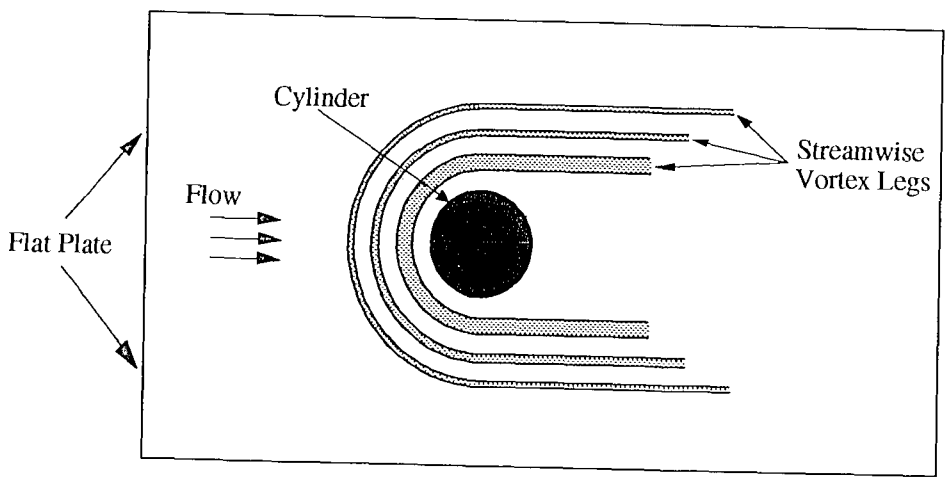

(b)

Figure 1.1 The Characteristic Triple "Horseshoe" or "Necklace" Vortex Pattern
(a) Oblique View
(b) Plan View

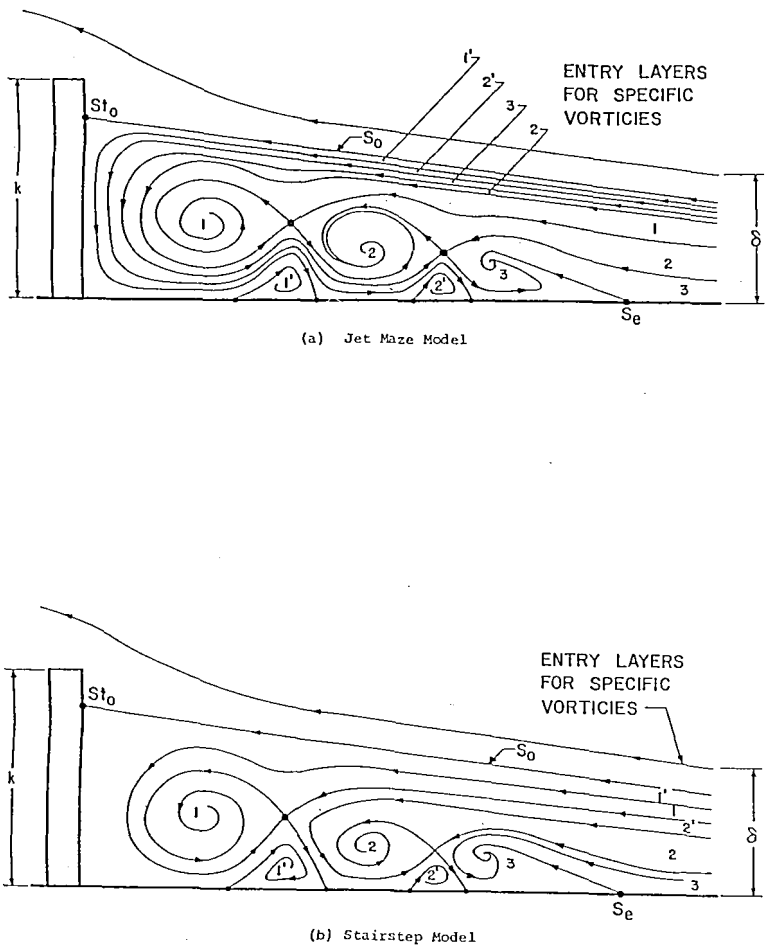

Figure 1.2 Three-Vortex Topologies of Norman (1972)
(a) Jet-Maze Topology
(b) Stairstep Topology

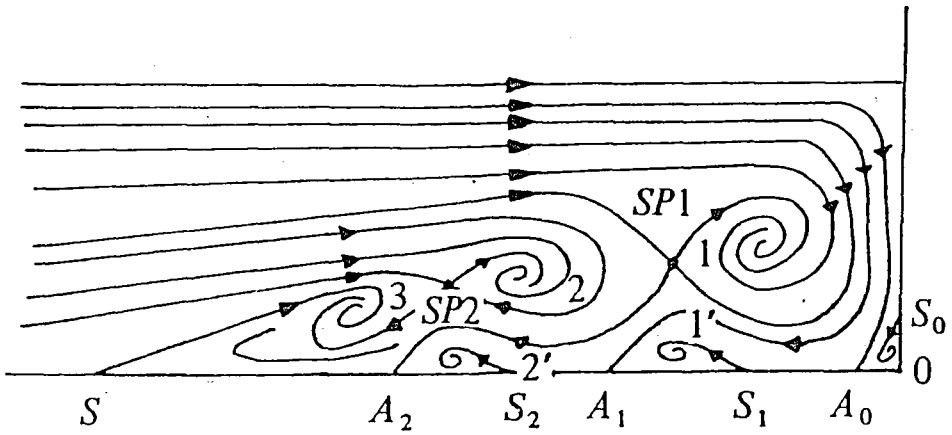

Laminar horseshoe vortex

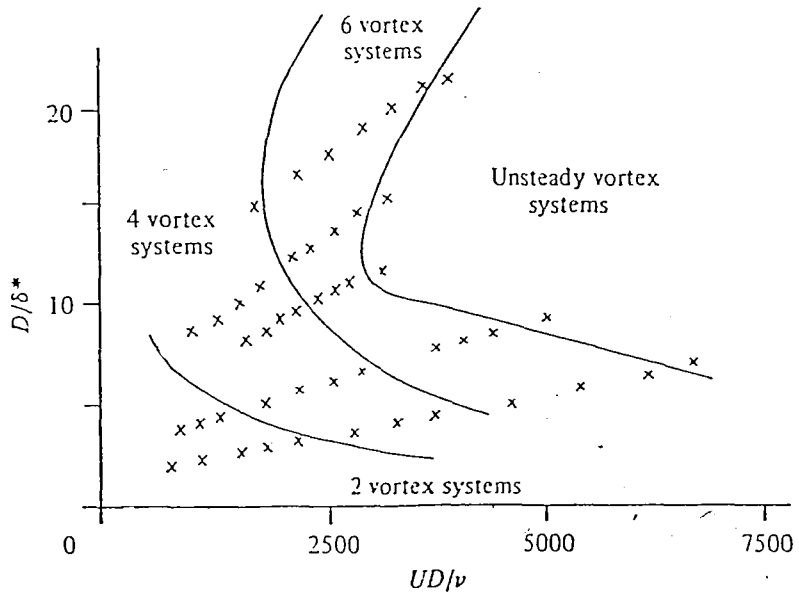

Figure 1.3 Results of Baker (1979)
(a) Steady, Laminar Three-Vortex Topology
(b) Plot of Re_D vs. D/δ^*

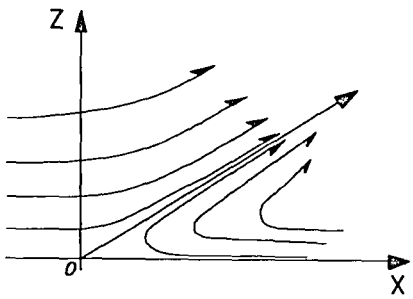

(a)

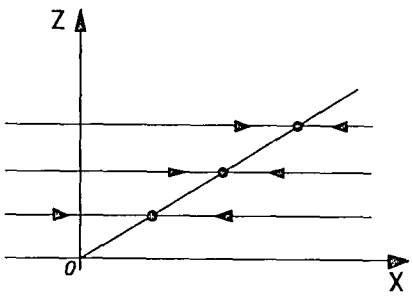

(b)

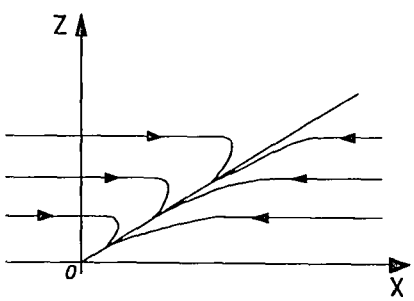

(c)

Figure 1.4 Three cases of symmetric, two-dimensional laminar flow separation
(a) x-z plane trajectories for $\eta_x/\xi_y > 1$;
(b) for $\eta_x/\xi_y = 1$;
(c) for $\eta_x/\xi_y < 1$

(Perry and Fairlie, 1974)

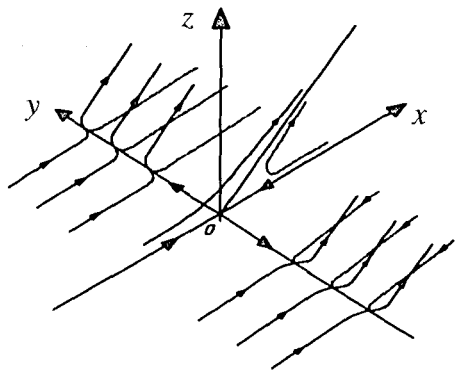

(a) Separation

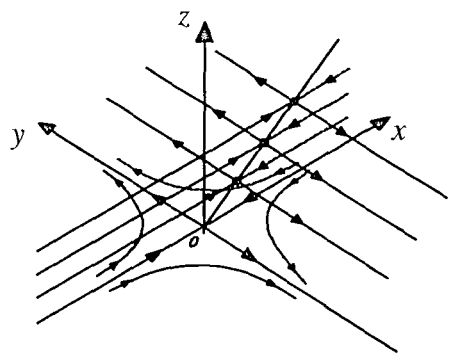

(b) Unstable Separation/Attachment

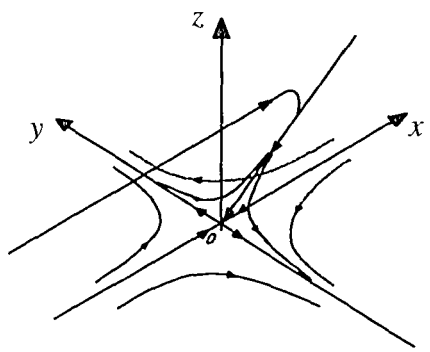

(c) Attachment

Figure 1.5 Oblique view (isometric projection) of symmetric, three-dimensional laminar flow separation.
(a) $\eta_x/\xi_y > 1$; (b) $\eta_x/\xi_y = 1$; (c) $\eta_x/\xi_y < 1$
(Perry and Fairlie, 1974)

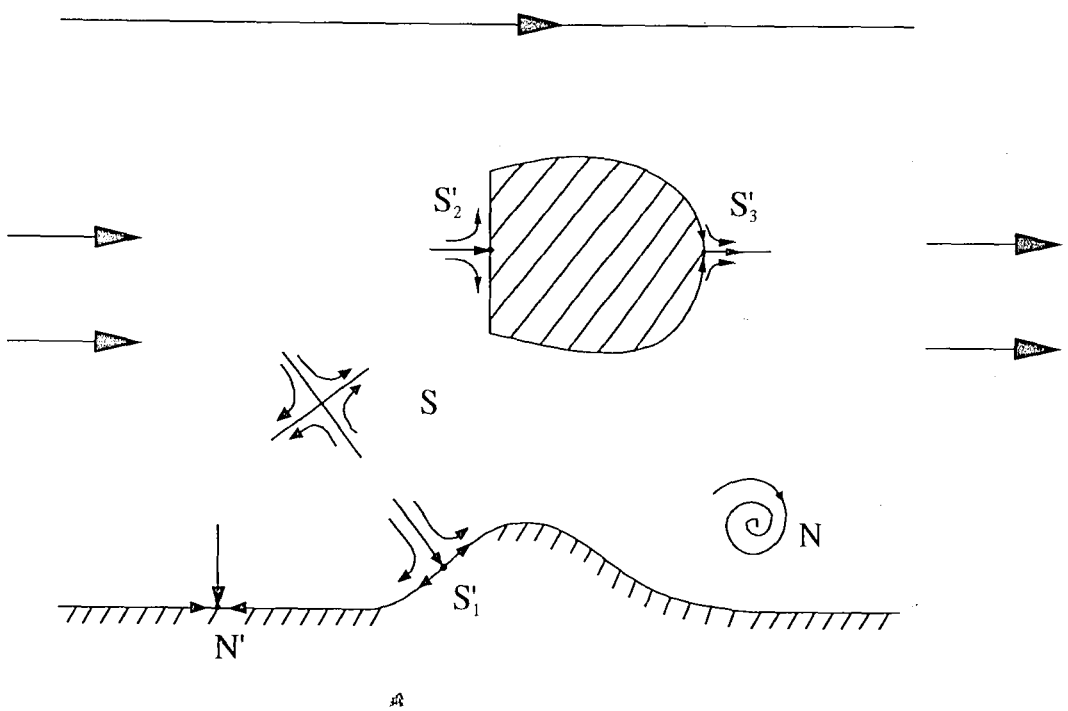

Figure 1.6 Saddle points and nodes in the streamline pattern on a section through the flow, denoted by S (saddles), N (nodes) in the flow and S′ (half-saddles), N′ (half-nodes) on the surfaces.

(Hunt, et al. 1978)

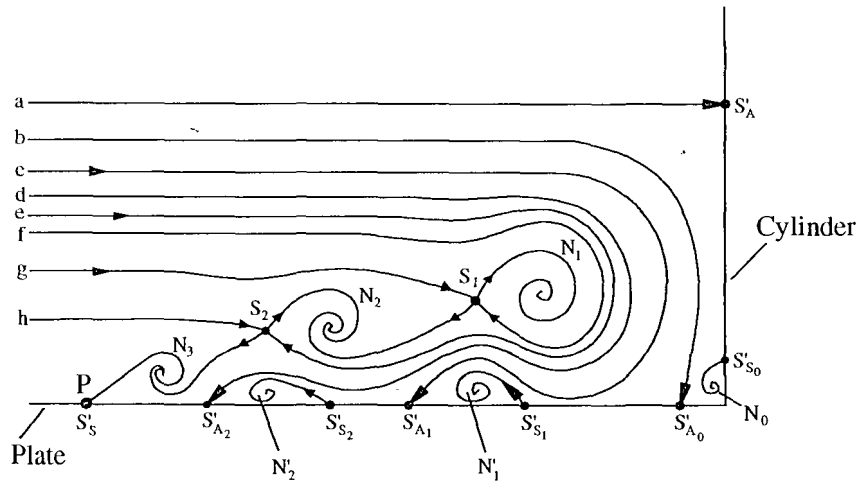

(a)

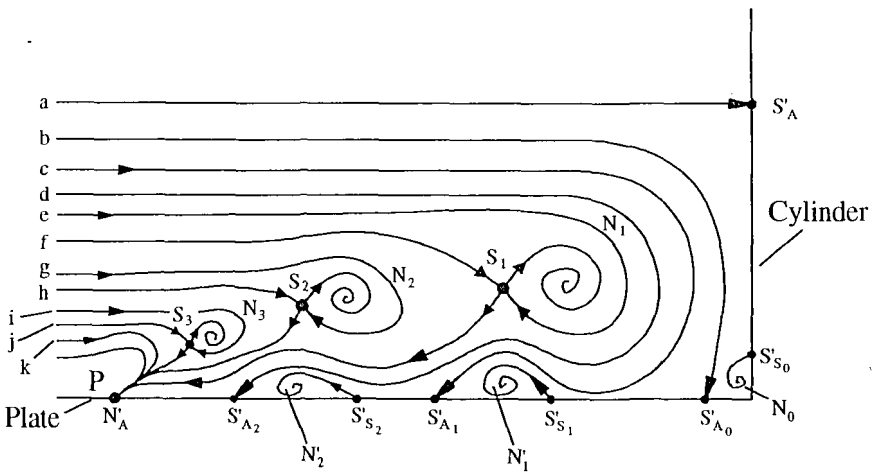

(b)

Figure 1.7 Steady, Laminar Three-Vortex Topologies of Visbal (1991)
(a) Jet-Maze Topology
(b) Attachment Topology

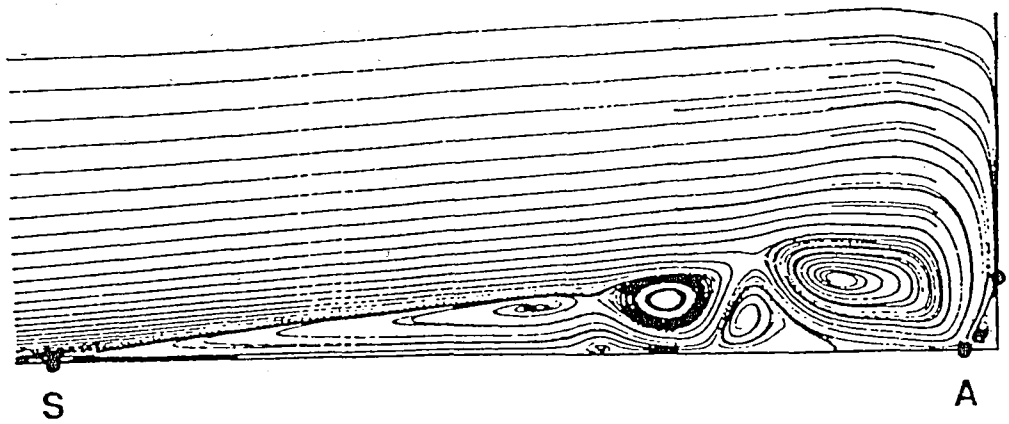

Figure 1.8 Computed Topology of Hung et al. (1991)
$Re_D = 1500$, $M_\infty = 2.0$

2.0 EXPERIMENTAL APPARATUS

2.1 Water Channel

Experiments were conducted in a recirculating, free-surface, Plexiglas water channel located in the Lehigh University Fluid Dynamics Research Laboratory. A plan-view schematic of the water channel is shown in Figure 2.1. The channel employs a 5 m long working section of 0.9 m width and 0.38 m depth. Water depth was maintained at approximately 0.29 m during these studies. Flow is driven by a horizontal, split-case, centrifugal pump powered by a Westinghouse variable-speed 7.5 horsepower, DC motor. Two 20-mesh, stainless steel, turbulence control screens and a 7.5 cm long, 0.8 cm cell honeycomb flow straightener establish undisturbed, uniform flow. A 2:1 inlet contraction further reduced the turbulence level in the working section $(u'/u_\infty \cong 0.2\%)$. Employing a tachometer feedback motor control, stable flows from 0.01 m/s to 0.4 m/s are achieved.

To maintain clean, algae and particulate-free water, the test section water was recirculated through 1 micron (μm) cotton-wound filters. To control the growth of algae and bacteria, liquid swimming pool chlorine (65% chlorine by volume) is added in concentrations of 0.007 g/liter to the water every three to four days. After filling the water channel, the water is circulated approximately five to seven days to facilitate deaeration and to allow the water temperature to reach equilibrium.

2.2 Test Plate and Cylinders

All cylinder studies were conducted on a 2.6 m long, 12 mm thick, flat plate with 5:1 elliptical leading edge. During all experiments, the plate was located 1.5 m downstream from the beginning of the working section to avoid spanwise flow variation

due to the channel contraction section. The plate is supported 10 cm above the channel floor by four sets of three spanwise legs to avoid the influence of the channel floor boundary layer. A standard Blasius flat plate solution, shown by Taylor (1990) to reflect empirical results within 5% for the present flat-plate test section, is used to establish local boundary layer thickness. A range of boundary layer thicknesses from 0.1 cm to 2.1 cm could be developed with this flat-plate test section.

Cylinders of diameters 2.5 cm, 4.8 cm, and 6.0 cm were used in this study to provide a range of geometric parameters, providing parametric overlap of Re_D, Re_{δ^*} and D/δ^* for cross-comparison of flow behavior. The cylinders were located on the plate centerline to preserve symmetry and to avoid interaction with the channel side-wall boundary layers. Since drag is minimal for the flow speeds employed for this study, the cylinders are simply set on the surface of the flat plate; special mounting or support methods are not necessary. The cylinder end-faces were carefully machined to negate leakage beneath the cylinder-plate junction; detailed dye studies verified that no junction leakage occurred.

2.3 Traversing Platform

A traversing platform that can be positioned over the entire length of the working section of the channel was used for all flow visualization studies. The platform, shown in Figures 2.2 and 2.3, traverses along two 4.1 m long cylindrical steel rails supported by mounts located at 0.3 m intervals on each side of the channel frame. A one-horsepower Reliance Electric motor can drive the platform over a range of speeds from 0.01 m/s to 0.24 m/s in either direction. Observation cameras mounted on the platform can be easily and accurately positioned at any location within the working section of the channel,

although the precise positioning of hydrogen bubble visualization probes is the platform's primary function.

2.4 Hydrogen Bubble Visualization

Hydrogen bubble visualization was employed exclusively to visualize the flow and characterize the topological structures examined in this study. As described by Clutter and Smith (1961) and Schraub et al. (1965), this technique employs an electrolytic process to generate either hydrogen bubble time lines or hydrogen bubble sheets, the deformation of which characterize and visualize local flow structure. In the present study, a 25μm platinum wire was used as the cathode and a 0.6 cm carbon rod as the anode in the electrolysis circuit. The wire, approximately 10-15 cm in length, is soldered to the legs or struts of a hydrogen bubble probe, fashioned from brass rods joined in various orientations depending on experimental demands; the probe supports are insulated using liquid electrical tape to assure bubble generation only at the wire. The probe arrangement employed for this study is shown in Figure 2.4.

A specially designed, high-voltage hydrogen bubble generator with an adjustable pulse duration and frequency is used to generate the bubble sheets, with hydrogen bubbles generated at the wire (cathode) and oxygen bubbles at the carbon rod (anode). Hydrogen bubbles are preferred over oxygen bubbles as tracers since volumetrically twice as much hydrogen is formed as oxygen during the electrolysis of water. The platinum wire generates extremely fine bubbles of approximately one-half wire the diameter (12μm), which are of minimal buoyancy for most flows. The buoyancy is dependent on bubble size, which in turn is dependent on the current between the anode and the cathode.

Pulsing the current density through the bubble wire generates fine time-lines of hydrogen bubbles which move with the flow, illustrating local spatial-temporal behavior. Sodium sulfate ($Na_2 SO_4$) is added in concentrations of 0.15 g/liter to the water to increase the number of free ions and reduce the potential difference necessary to generate an appropriate hydrogen bubble density. A schematic of the visualization system is shown in Figure 2.5. Details of the construction of the probes and the voltage generator are described in Metzler (1980).

2.5 Video System

An S-VHS video system was used to record flow visualization information obtained during this study. The video system includes a Panasonic AG-7300 heavy-duty editing video cassette recorder along with a high-resolution SONY Trinitron PVM-1344Q color video monitor, and a high-resolution SONY SSC-S20 CCD (Charge Coupled Device) color video camera with 460 line resolution and S-VHS capability. Video data was recorded in the S-VHS mode and could be played back in real time or 0 to 1000% of real time, forward or reverse. This capability allowed detailed study of recordings, and acquisition of single-frame scenes using a color frame grabber. Details of the color frame grabber are not addressed since it was only used to obtain video reproductions for purposes of illustration.

2.6 Laser System for Flow Visualization

A laser sheet illumination process was employed for illumination of the hydrogen bubble visualization. A 1 mm thick laser light sheet is generated with a LEXEL, 10-Watt Argon Ion Laser operating in conjunction with a scanning mirror. As illustrated in Figure 2.6, the incident laser beam is reflected by a 90° turning mirror, passes through a

focusing singlet lens, is reflected 90° again, impinging onto a frequency- and amplitude-controlled, oscillating scanning mirror which creates the scanned light sheet. The singlet lens and the mirrors are mounted on a laser table that traverses the entire working section of the channel. The scanning frequency of the mirror can be varied over a range of 5 Hz to 400 Hz; for the flow visualization work, the scanning frequency was kept at approximately 150 Hz to avoid interference with the 60 Hz framing-rate of the video camera.

2.7 Visualization Techniques

Flow visualization during this study was arduous due to the inherent three-dimensionality, small scales, and sensitivity of the flow structures examined. Great care had to be exercised in the generation of the hydrogen bubbles: if the bubble density was too great, this would cause the flow structures to destabilize, thus biasing the results; if the bubble density was too low, an accurate assessment of the flow structure behavior would be difficult. For example, if the current density from the generator was too high, the bubble density could interfere with the feeding layers and cause the break down of sensitive topological flow structures. Additional care also had to be exercised in choosing the proper length of bubble wire. The wire length must be between three and four cylinder diameters in length to remove disturbances created by vortex shedding from the struts of the hydrogen bubble probe from the proximity of the juncture vortices under study. Wires below this length proved to be problematic. Wires exceeding this length would create high bubble concentrations outside the symmetry plane, obstructing the view of the flow structures due to extraneous bubbles.

A great number of 'practice' runs were necessary to determine the optimum bubble density, current density, and wire length necessary to illustrate the vortex

dynamics. Once a satisfactory wire length and current density were established, experiments could proceed with confidence in the observed results. As shown in Figures 2.2 & 2.3, side and plan views are obtained by employing cameras mounted on either the traversing platform or tripods located adjacent to the channel.

The 1 mm thick laser sheet lighting was critical in allowing the videographic recording of the intricate details of the flow structures. Black posterboard was attached to the side-walls and floors of the channel to provide a maximum contrast between the laser-illuminated bubbles and the background. The thin, high-intensity laser sheet allowed optimal illumination of two-dimensional cross-sections of the flow structures, and increased the bubble tracking capability of the video camera. The aforementioned precautions are necessary since hydrogen bubbles are soluble in water and are rapidly absorbed, which has both advantages and disadvantages. The primary advantage is that the bubbles do not return or accumulate in recirculating regions, and thus interfere with or obscure local flow processes. The disadvantage is that the half-life of the bubbles is short (on the order of 3 seconds), which limits the time over which they are effective visualization agents. The use of smaller diameter cylinders, which result in smaller, higher-frequency flow structures, helped overcome half-life problems. If the cylinder diameter was large, the bubbles might be absorbed before they navigated the entire flow structure; if the cylinder diameter was too small, bubble accumulation could destabilize the local flow, thus modifying the sensitive flow structure under scrutiny.

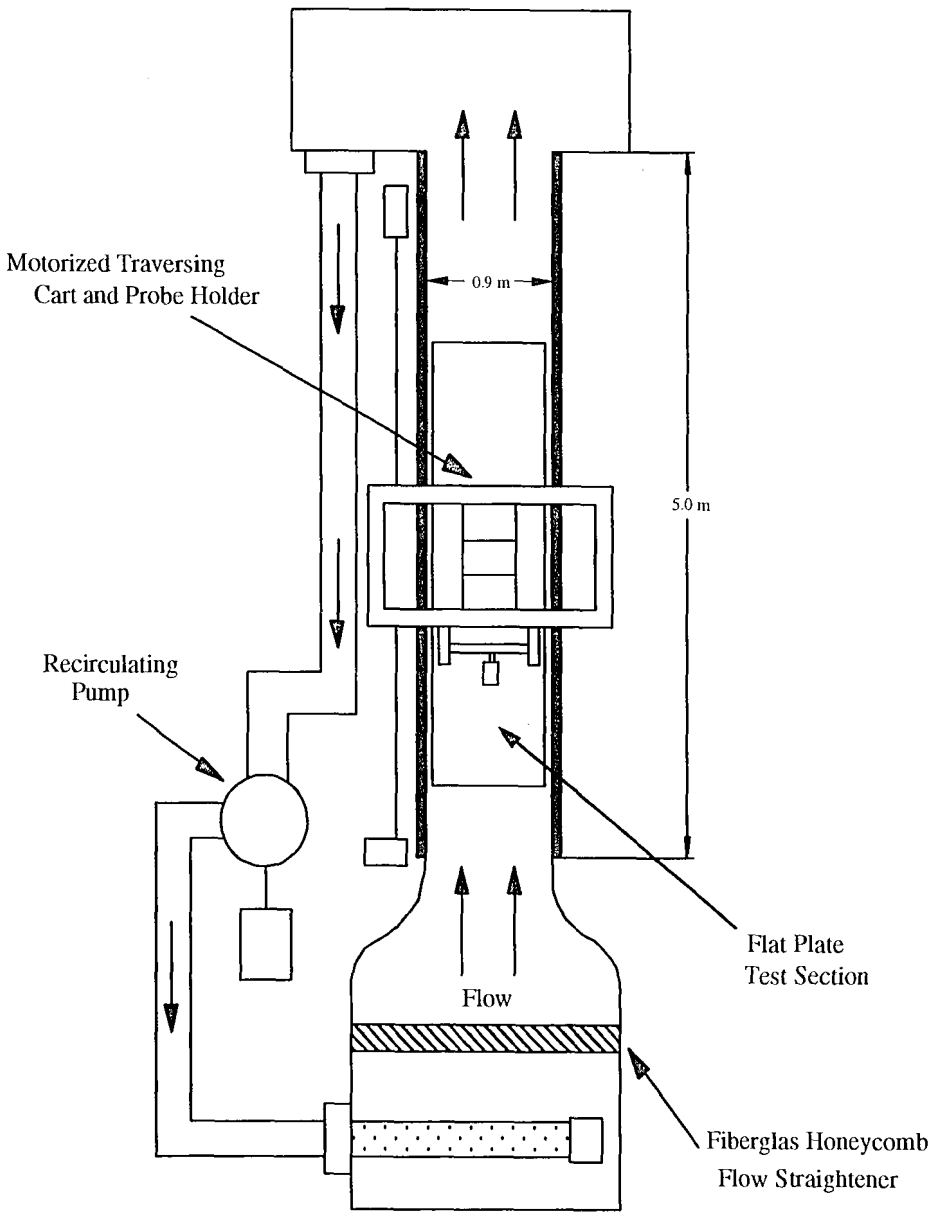

Figure 2.1 Plan View of Water Channel

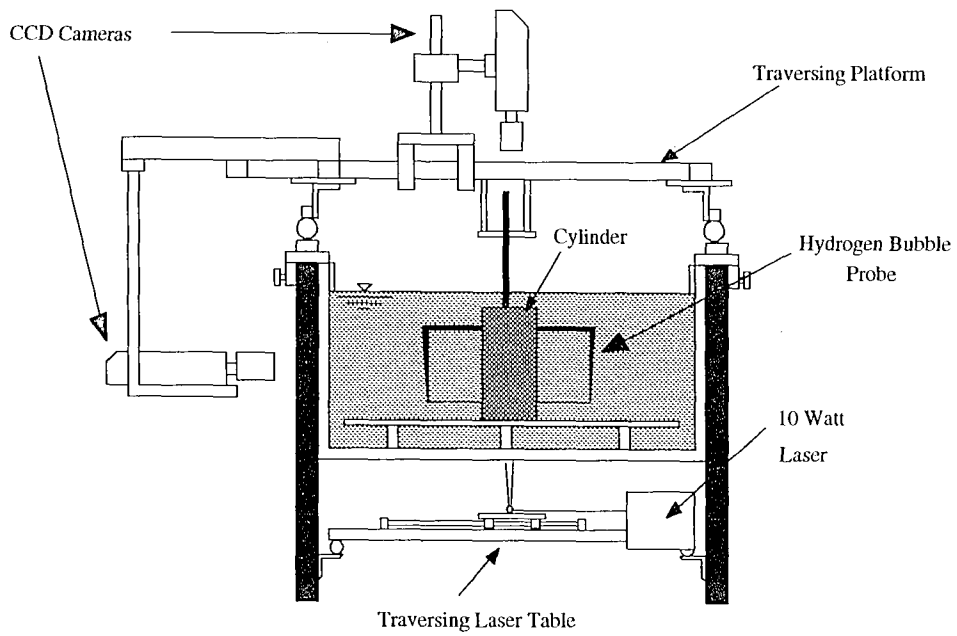

Figure 2.2 Front View of Water Channel with Traversing Platform

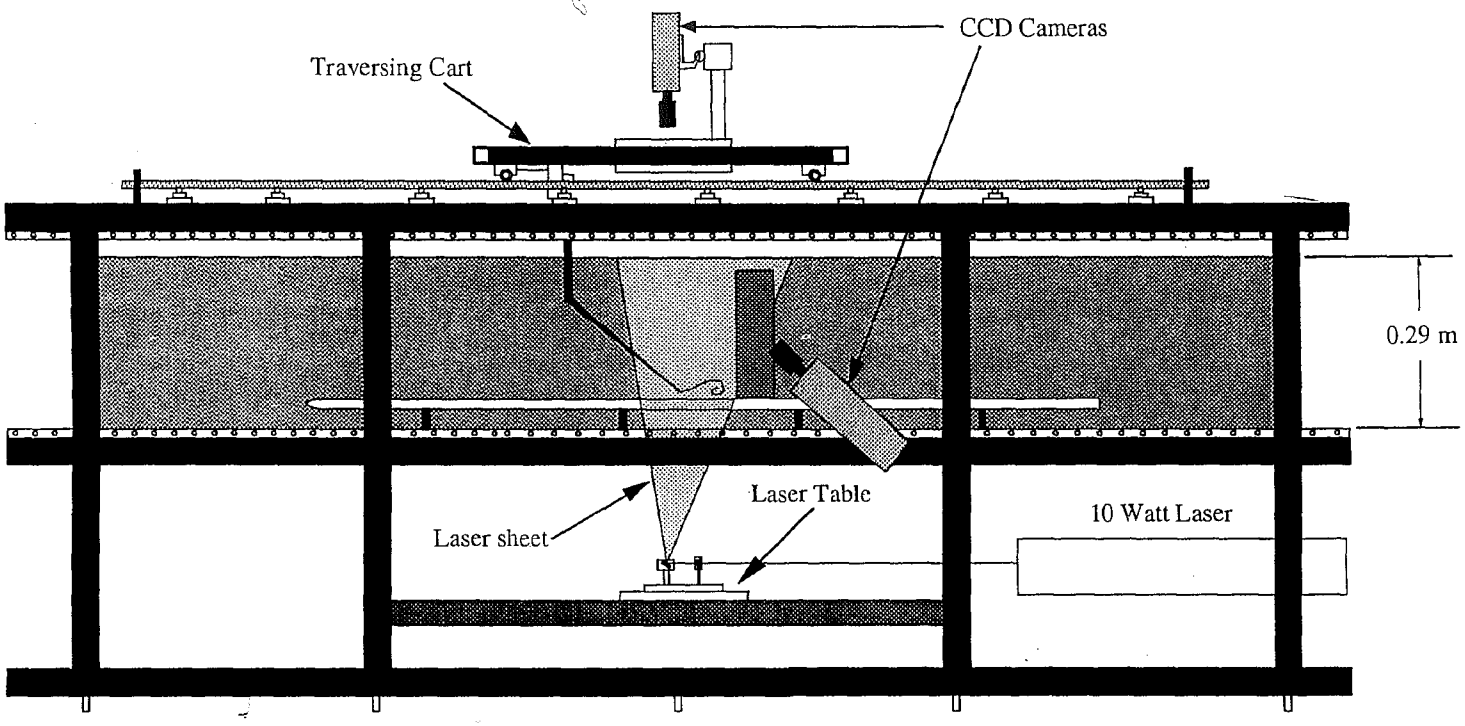

Figure 2.4 Side View of Water Channel

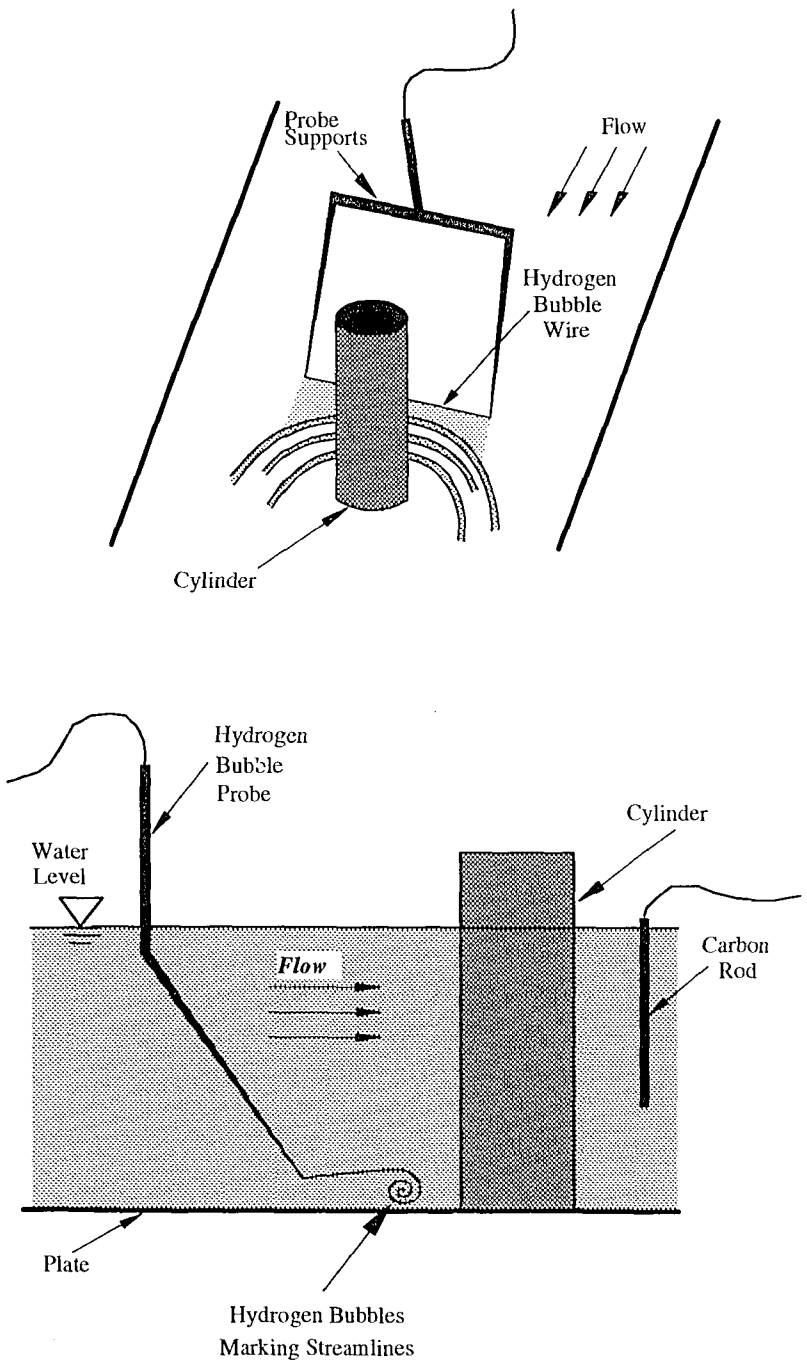

Figure 2.4 Hydrogen Bubble Probe Arrangements

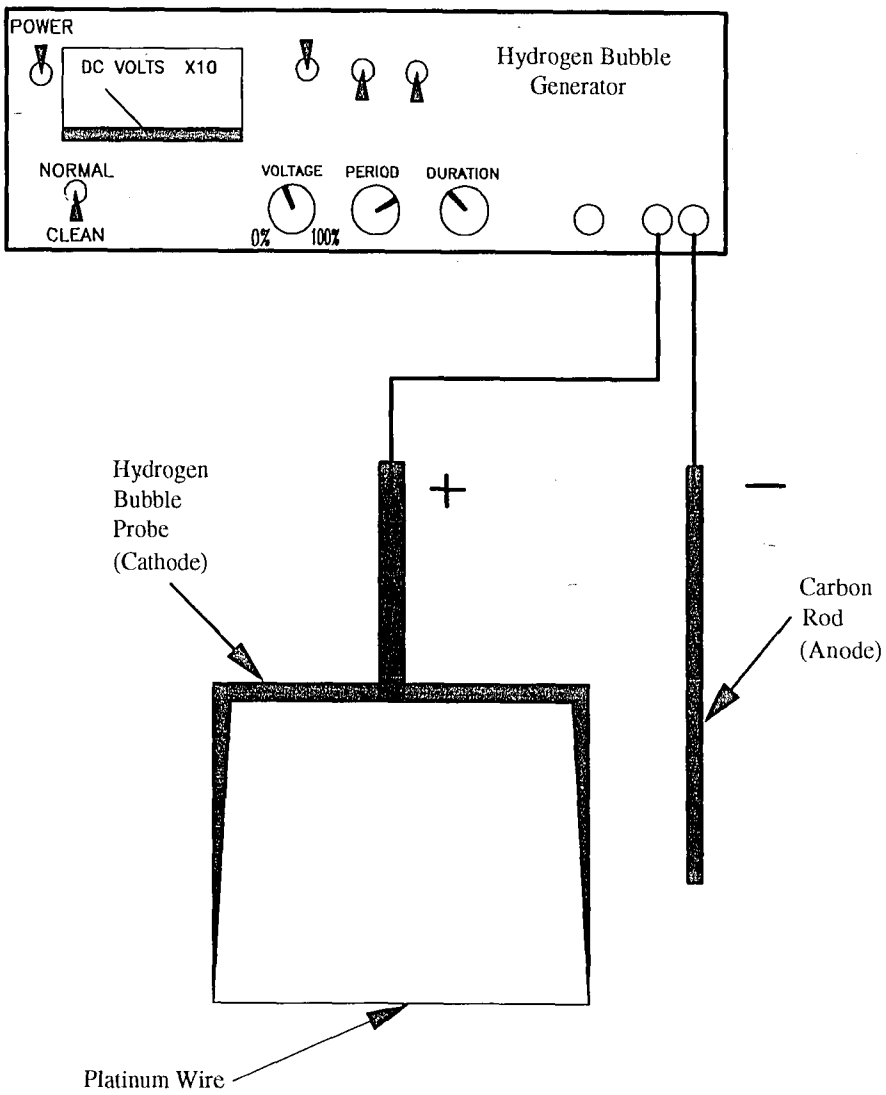

Figure 2.5 Hydrogen Bubble Probe and Generator

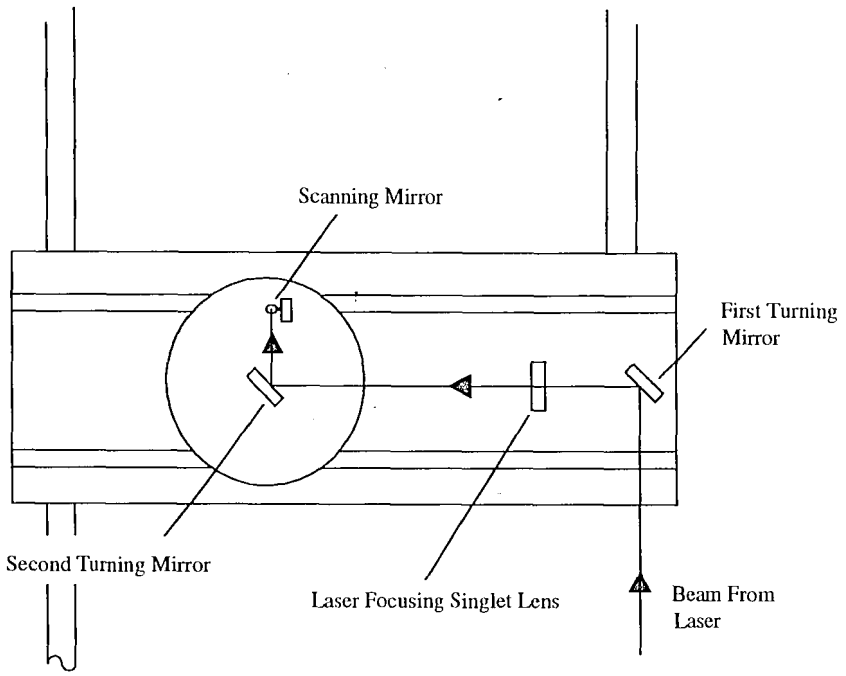

Plan-View

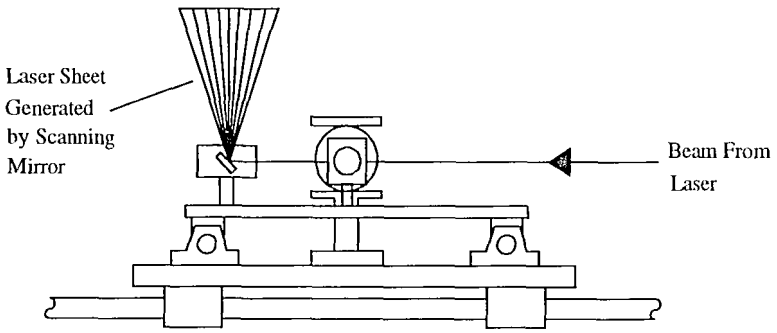

Side-View

Figure 2.6 Traversing Laser Table

3.0 EXPERIMENTAL RESULTS

3.1 Introduction.

The following chapter presents the results of the hydrogen bubble visualization study of the steady, laminar three-vortex system formed at a cylinder/flat-plate juncture. Attention is focused on the topological structure of the three-vortex system, consisting of critical point locations (separation/attachment of flow), and vortex 'feeding' through different shear layers (feeding streamlines) of the approach fluid. Due to the large local changes in the approach flow boundary layer caused by the adverse pressure gradient imposed by the cylinder, all boundary layer parameters (δ^*, Re_{δ^*}, etc.) are given as "undisturbed" parameters; these are based on the equivalent flat plate boundary layer for the same flat-plate location without the cylinder present. All dimensionless parameters are calculated from the Blasius boundary layer profile formula:

$$\frac{\delta^*}{x} = \frac{1.721}{Re_x^{1/2}} \tag{3.1}$$

based on the distance (x) from the leading edge of the flat plate to the leading edge of the cylinder, as shown in Figure 3.1

3.2 Observed Steady, Laminar Three-Vortex Topologies.

3.2.1 General Topological Characteristics of Juncture Flow.

As a flow approaches a cylinder/flat-plate juncture, it experiences a strong adverse pressure gradient due to the deceleration of the flow, which causes the approaching boundary layer velocity profile to develop an inflection, and undergo a symmetric local separation, forming a u-shaped region of separated flow bounded by a line of separation near the cylinder/flat-plate juncture. Over a specific range of Reynolds numbers (based on cylinder diameter and streamwise location), this inflectional profile

destabilizes, rolls-up, and forms a steady, laminar three-vortex system about the base of the cylinder. This resulting steady-flow phenomenon is a complex interaction of inertia, pressure and viscous forces in a delicate balance. Figure 3.2 shows 1) the general configuration of the steady, laminar three-vortex system which develops upstream of the cylinder/flat-plate juncture, 2) the coordinate system used in this study, and 3) the location of the laser sheet illumination used to track the hydrogen bubbles introduced into the flow.

Figure 3.3 is a 2-D streamline schematic of the standard Jet-Maze topology hypothesized by many researchers, including Norman (1972) and Sedney et al. (1975) as the only steady, laminar three-vortex topology for a cylinder/flat-plate juncture. Applying the notation of Hunt et al. (1978), where N denotes full-nodes, S denotes full-saddles, and the primed quantities are half-nodes and half-saddles, this system is basically comprised of three clockwise rotating (negative vorticity) main vortices (primary N_1, secondary N_2 and tertiary N_3), separated by three smaller counter-rotating (positive vorticity) vortices (N_1', N_2', and N_0) located adjacent to the plate. This particular three-vortex topology is additionally characterized by two free stagnation/saddle points (S_1 and S_2) and by a series of separation (S'_{S_0}, S'_{S_1}, S'_{S_2}, S'_S) and attachment (S'_{A_0}, S'_{A_1}, S'_{A_2}) points along the plate and cylinder. Here the subscripts "S" and "A" denote separation and attachment. Further details of the Jet-Maze topology including its streamline feeding characteristics and topological structure will be discussed in subsequent sections.

Particular attention is focused in this paper on the outermost separation point P, since a new type of steady, laminar three-vortex topology has been established experimentally, wherein this outermost point changes from a half-saddle point of separation to a half-saddle point of attachment. Note that the legs of all vortices, as well

as separation and attachment lines, deform around the cylinder and trail downstream in the streamwise direction, eventually destabilizing and breaking down in the wake of the cylinder.

3.2.2 Visualized Steady, Laminar Three-Vortex Topologies.

Three distinct steady, laminar three-vortex topologies were observed using hydrogen bubble visualization and are shown in 2-D streamline schematics in Figures 3.4a, b and c, along with the classification of all critical points. It was determined that each of these topologies comprises a separate, discreet parametric 'Regime' within a parameter space based on dimensionless parameters Re_D, and D/δ^*. The Regimes that were experimentally established in this study are: 1) a Regime 1 topology, Figure 3.4a, which is a new type of topology previously undetected, either experimentally or numerically; 2) a Regime 2 topology, Figure 3.4b, which is the standard Jet-Maze topology hypothesized by several searchers as the only steady, laminar three-vortex topology; and 3) a Regime 3 (Attachment) topology, Figure 3.4c, the topology, discovered computationally by Visbal (1991), and confirmed experimentally in this study. Subsequent sections will describe the individual topologies along with the details of the experimental determination process, including 'feeding' streamline characteristics. Special attention is focused on the Regime 3 (Attachment) topology, since its outermost point P is one of attachment (N'_A), unlike the points of separation (S'_S) found in the Regime 1 and Regime 2 topologies, a property which is counter-intuitive for juncture flows of this type.

In Chapter 4, each topology is compared and contrasted with the standard Jet-Maze topology as well as other previously conjectured topologies. In addition, each

steady, laminar three-vortex topology are also examined using critical-point concepts to verify the character and validity of the topological structure.

3.2.3 Mapping of Parameters Determining Flow Regimes.

No single functional relationship or nondimensional parameter could be established which will predict which flow Regime will be present under particular conditions. Flow Regimes appeared to be functions of free-stream velocity, boundary layer thickness, fluid viscosity, and cylinder diameter. Dimensionless analysis suggests a dual functionality of the Regimes on D/δ^* and Re_D. To examine this functionality, mappings of the transition bounding lines between the respective flow Regimes as functions of D/δ^* and Re_D were constructed using data for all three cylinders over a range of velocities and locations. Figure 3.5 is a mapping of all points of flow Regime transition over a range of flow parameters; it appears that Re_D and D/δ^* do a reasonable job of characterizing the Regime behavior. The data is displayed with open ends at the top and bottom indicating that the steady, laminar three-vortex system can exist outside the range of the present results; however, these regions could not be mapped due to limitations of both the flow range of the water channel and the hydrogen bubble flow visualization method. Details of the cylinder/flat-plate juncture flow regimes, other than the regimes examined in this study, are described in detail by Baker (1979) and Greco (1990).

3.3 Regime 1 Topology.

For large values of Re_D and D/δ^*, Regime 1 occurs over the parametric region shown in Figure 3.6. For the present test system, these parametric values corresponded to cylinder locations in close proximity to the leading edge of the flat-plate, and free-

stream velocities between 4.5 and 8.7 cm/s. Figure 3.7a is a 2-D streamline schematic of the Regime 1 topology on the symmetry plane with additional classification of all its critical points; Figures 3.7b and c are side-view hydrogen bubble visualization photographs of the Regime 1 topology for the 4.8 cm diameter cylinder with $D/\delta^* = 36$ and $Re_D = 4150$. It will be shown that these two photographs demonstrate the uniqueness of the Regime 1 topology and its distinction from other steady, laminar three-vortex topologies. The locations of pertinent critical points are indicated in Figures 3.7b and c to facilitate a comparison between the hydrogen bubble photographs and the streamline schematic of Figure 3.7a. The most significant characteristic of the Regime 1 topology that distinguishes it from other possible topologies lies in the connecting streamline between the two free stagnation/saddle points S_1 and S_2. This can be seen in Figure 3.7a by following streamline 'e' from left to right. The flow along streamline 'e' navigates around the edge of the primary vortex N_1, reflects off saddle point S_1 to saddle point S_2, subsequently reflecting off S_2 and feeds directly into the tertiary vortex N_3.

3.3.1 Experimental Determination of Regime 1 Topology.

Differentiation of the Regime 1 topology from other steady, laminar three-vortex topologies required careful examination of the flow along several different streamlines. Experimentally, this was done by introducing the hydrogen bubble sheets at a series of different feeding heights relative to the flat-plate surface. Since the flow is steady, the streaklines created by the hydrogen bubbles will be coincident with the streamlines of the flow.

In Figure 3.7b, the tertiary vortex N_3 is marked by hydrogen bubbles fed into the flow along a selected streamline using a spanwise hydrogen bubble wire located approximately 6.0 cm upstream of the cylinder/plate junction and 1.5 cm above the plate.

Comparing this pattern with the 2-D streamline schematic of Figure 3.7a, the hydrogen bubbles are feeding essentially along streamline 'e,' as also indicated in Figure 3.7b. As indicated in the 2-D streamline schematic, the flow navigates around the primary vortex N_1, reflects first off saddle point S_1, then off saddle point S_2, and then feeds tertiary vortex N_3. But this feeding height alone is not sufficient to conclusively differentiate between the Regime 1 topology and other possible three-vortex topologies. In Figure 3.7c, the bubble wire was lowered to a height of 1.2 cm above the plate and bubbles fed along streamline 'f,' as indicated. Following streamline 'f' in Figure 3.7c, the streamline reflects off saddle point S_1, heads upstream to next reflect off saddle point S_2, and again feeds the tertiary vortex N_3.

To examine the effect of cylinder height (h) on the flow topology, a squat-cylinder was employed with the dimensions D = 4.8 cm and h = 1.5 cm (aspect ratio $h/D = 0.31$); illustration of a streamline feeding pattern is shown in Figure 3.8 for the flow conditions $D/\delta^* = 32$ and $Re_D = 4000$. The streamlines proved difficult to feed for this cylinder due to a decrease in overall size of the three-vortex system by a factor of three relative to the cylinder diameter, but the results indicated that there were essentially no topological changes induced by a change in cylinder height. However, as shown, the overall shape of the steady, laminar three-vortex topology for the squat-cylinder is somewhat compressed in the flow direction and the main vortices are square-like in shape compared to the elliptic/circular shape of the topological flow patterns for large aspect ratio cylinders (Figures 3.7b & c). Other than overall size and shape changes, the streamline feeding characteristics (topological structure) remains the same for the squat cylinder.

3.4 Regime 2 (Jet-Maze) Topology.

The Regime 2 topology is the standard Jet-Maze topology identified by many researchers, and previously considered as the only steady, laminar three-vortex topology for a cylinder/flat-plate geometry. As the shaded region of Figure 3.9 indicates, the Regime 2 (Jet-Maze) topology exists in "natural" form between the Regime 1 and Regime 3 topologies. The selection of the term "natural" and its use will be explained in detail in subsequent sections. The transition to the Regime 2 topology occurs abruptly as a function of Re_D and D/δ^*. For example, if D/δ^* is held constant at 25, and Re_D is changed slowly from 2500 to 3500, the flow topology will switch almost instantly from the Regime 1 topology to the Regime 2 (Jet-Maze) topology as a critical Re_D is exceeded at approximately $Re_D = 2800$; this switch appears to be a clean transition, with no observable fluctuations between Regimes once the parameter boundary is crossed.

As mentioned previously in section 2.7, great care had to be exercised in the generation of hydrogen bubbles used in the visualization, for if the bubble density was too great, the steady, laminar three-vortex topology would destabilize, biasing the results. However, the Regime 2 (Jet-Maze) topology was found to be the most "stable" topology of all three topologies established in this study and was relatively insensitive to the presence of the hydrogen bubbles and disturbances in the flow field. In contrast, both the Regime 1 and Regime 3 topologies will destabilize and break down to a Regime 2 (Jet-Maze) topology in the presence of any significant disturbance or perturbation in the flow field. Further characterization of this sensitivity will be discussed in Chapter 4.

As Re_D and D/δ^* decrease, the Regime 2 topology can become unsteady, and begin a random, low frequency fluctuation between Regimes 2 and 3; this narrow regime of unsteady behavior is indicated by the dark gray band in Figure 3.9. However, once the bounding line between the Regime 2 and Regime 3 topologies is crossed, the Regime

3 topology will stabilize. Details of this transition regime will be considered in the following section.

3.4.1 Experimental Determination of the Regime 2 (Jet-Maze) Topology.

The same experimental procedure described in section 3.3.1 was applied to examine the characteristics of the Regime 2 topology. As before, in order to identify the topological behavior, detailed examination was done of the two main streamlines which reflect off the full-saddle point S_1. Figure 3.10a shows the 2-D streamline schematic of the Regime 2 (Jet-Maze) topology, and Figure 3.10b and c show side-view hydrogen bubble visualization photographs of the Regime 2 (Jet-Maze) topology for the 6.0 cm cylinder at $D/\delta^* = 18$ and $Re_D = 2250$. In Figure 3.10b, the hydrogen bubble wire, located approximately 5.0 cm upstream of the cylinder/plate junction and 1.7 cm above the plate, is feeding bubbles along the streamline 'e' indicated in Figure 3.10a. As Figure 3.10b shows, streamline 'e' circumvents the primary vortex N_1, reflects off saddle point S_1 and feeds vortex N_2. Vortex N_3 is fed as well since 'e-f' is a very narrow shear layer and it was difficult to feed only the secondary vortex N_2 from overtop along streamline 'e.' In Figure 3.10c, the hydrogen bubble probe is at a height of 1.2 cm above the plate such that the bubbles are fed along streamline 'g.' The bubbles reflect off saddle point S_1 and feed directly into vortices N_1 and N_2, a standard Jet-Maze feeding characteristic. Recall that for the Regime 1 topology, the hydrogen bubbles, after reflecting off saddle point S_1, navigated around the secondary vortex N_2 to feed the tertiary vortex N_3 (Figure 3.7b). Further comparison and contrast of all three Regime topologies will discussed in detail in Chapter 4.

As mentioned previously in section 3.4, for lower values of D/δ^* and Re_D, the Regime 2 (Jet-Maze) topology will become unsteady and begin to fluctuate randomly at

very low frequencies between the Regime 2 and Regime 3 topologies. In effect, the Regime 2 (Jet-Maze) topology switches intermittently to the Regime 3 (Attachment) topology; during this switch, the outermost critical point changes from a half-saddle point of separation (S'_S) to a half-nodal point of attachment (N'_A). Figure 3.11 illustrates this unusual random switching behavior in a five-step sequence. In step 1, the Regime 3 (Attachment) topology is initially present and is indicated by the streamline reflecting upstream off saddle point S_1, bypassing both the secondary vortex N_2 and the tertiary vortex N_3. In step 2, Regime 3 begins to switch to Regime 2 (Jet-Maze) topology as indicated by the arrow pointing to saddle point S_2. The feeding streamline changes direction at saddle point S_2 and begins to feed into the secondary vortex N_2 during steps 3 and 4, which is a characteristic of a Regime 2 (Jet-Maze) topology. Lastly, by step 5, the feeding streamline changes direction once again at saddle point S_2, and begins to feed back around vortex N_2 and back toward the half-nodal point of attachment N'_A, shifting back to Regime 3. Note that this regime switching process is not periodic; the process appears to be random, with no discernible frequency, with neither Regime 2 nor Regime 3 dominating.

Once the boundary between the Regime 2 and Regime 3 topologies is crossed, this fluctuating behavior ceases and the steady, laminar three-vortex Regime 3 topology persists.

3.5 Regime 3 (Attachment) Topology.

The Regime 3 (Attachment) topology is a new type of steady, laminar three-vortex topology, originally discovered computationally by Visbal (1991). For this new topology, the outermost line of coalescence (point P) is line of attachment (N'_A) rather than a line of separation (S'_S) as is the case for Regime 1 and Regime 2 (Jet-Maze)

topologies. The fluid above the surface flows into the critical point P, not out; hence, the point P is an attachment point, not a saddle point of separation. Another significant difference is the presence of an additional critical point, reflected by a full saddle point (S_3) in the flow associated with the tertiary vortex N_3. As the shaded region of Figure 3.12 indicates, the Regime 3 topology only develops for large boundary layer displacement thicknesses and low Re_D.

3.5.1 Experimental Determination of the Regime 3 (Attachment) Topology.

The Regime 3 (Attachment) topology proved to be the most problematical topology to feed as well as the most vulnerable to flow disturbances. The reasons for this are twofold: 1) the free-stream velocities associated with the presence of the Regime 3 topology are low, which allows the potential for the hydrogen bubbles to rise and/or be reabsorbed, and 2) greater amounts of bubbles were required in order to feed back and to visualize the attachment point N'_A, which could create a flow disturbance causing immediate breakdown of the Regime 3 topology to the Regime 2 (Jet-Maze) topology. Figure 3.13a shows the 2-D streamline schematic of the Regime 3 topology; Figures 3.13b and c are side-view hydrogen bubble visualization photographs of the Regime 3 topology for the 4.8 cm cylinder at $D/\delta^* = 7$ and $Re_D = 1960$. Upon closer inspection of Figure 3.14a, one can contrast the feeding characteristics and topological structure of this new topology with those of the Regime 1 and Regime 2 topologies. These differences will be discussed in detail in Chapter 4.

Once again, the same experimental process employed for the Regime 1 and Regime 2 (Jet-Maze) topologies is utilized to establish the topological structure of the Regime 3 topology, examples of which are shown in Figures 3.13b and c. In Figure 3.13b, the hydrogen bubble wire, located approximately 7.0 cm upstream of the

cylinder/plate junction and 2.0 cm above the plate, feeds bubbles along streamline 'e' in Figure 3.13a. As shown, streamline 'e' navigates around primary vortex N_1, reflects off saddle point S_1 (partially feeding primary vortex N_1), and feeds back upstream between secondary vortex N_2 and counter-rotating vortex N_1', feeding back to the half-node attachment point N_A'. It is not clear from the photographs that the bubbles are attaching to the flat-plate at the half-nodal point of attachment (N_A'), but such attachment was discernible by the naked eye. Good visualization of the attachment point was complicated by the rise and/or reabsorbtion of the bubbles in the vicinity of the attachment point due to the extremely low velocities associated with the attaching flow. To feed streamline 'f,' the hydrogen bubble probe is lowered to a height of 1.4 cm as shown in Figure 3.13c. In this Figure, streamline 'f' also reflects off saddle point S_1 (partially feeding primary vortex N_1), and becomes coincident with streamline 'e,' feeding between secondary vortex N_2 and counter-rotating vortex N_1', back to the half-node attachment point N_A'.

As mentioned previously, it is not clear from the photographs (Figures 3.13b and c) that the hydrogen bubbles are flowing to the attachment point N_A', but this could be distinguished in the actual experiment. Effective pictures could not be taken of the actual approach of the bubbles to attachment point N_A' because the bubbles were rapidly reabsorbed in the very slow moving fluid in and around the attachment point. Due to the sensitivity of the Regime 3 topology to any kind of flow disturbance, smaller amounts bubbles had to be generated at the wire to keep the topology from breaking down into the standard Jet-Maze (Regime 2) topology. While the migration of bubbles to the attachment point N_A' could be observed by eye, effective photography of the migration was not possible due to the low concentration of bubbles. The tertiary vortex N_3 proved impossible to feed due to its low rotational speed (low circulation) and also due to the

disruptive effect of the hydrogen bubbles when introduced in close proximity of the attachment point N'_A. By approximately $D/\delta^* = 4$ and $Re_D = 1400$, the free-stream velocity was so low that the hydrogen bubbles were rendered ineffective for further discrimination of the Regime 3 topology.

Note that for the Regime 3 topology the feeding order of the main vortices followed a simple pattern. Starting at the upper portion of the boundary layer and traversing downwards, the main vortices are fed in a step-wise fashion: first N_1, then N_2, and lastly N_3, a behavior that is similar to the Stairstep topology proposed by Norman. Further comparison of the Regime 3 topology and other hypothesized topologies is done in Chapter 4.

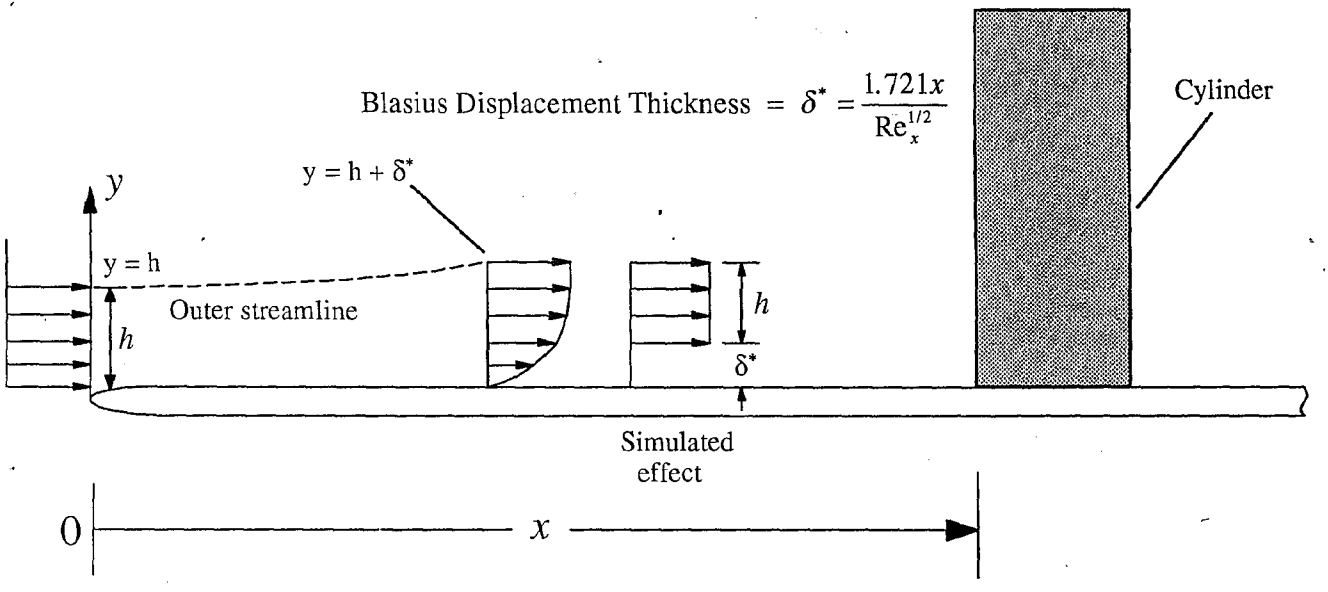

Figure 3.1 Definintion of δ^*

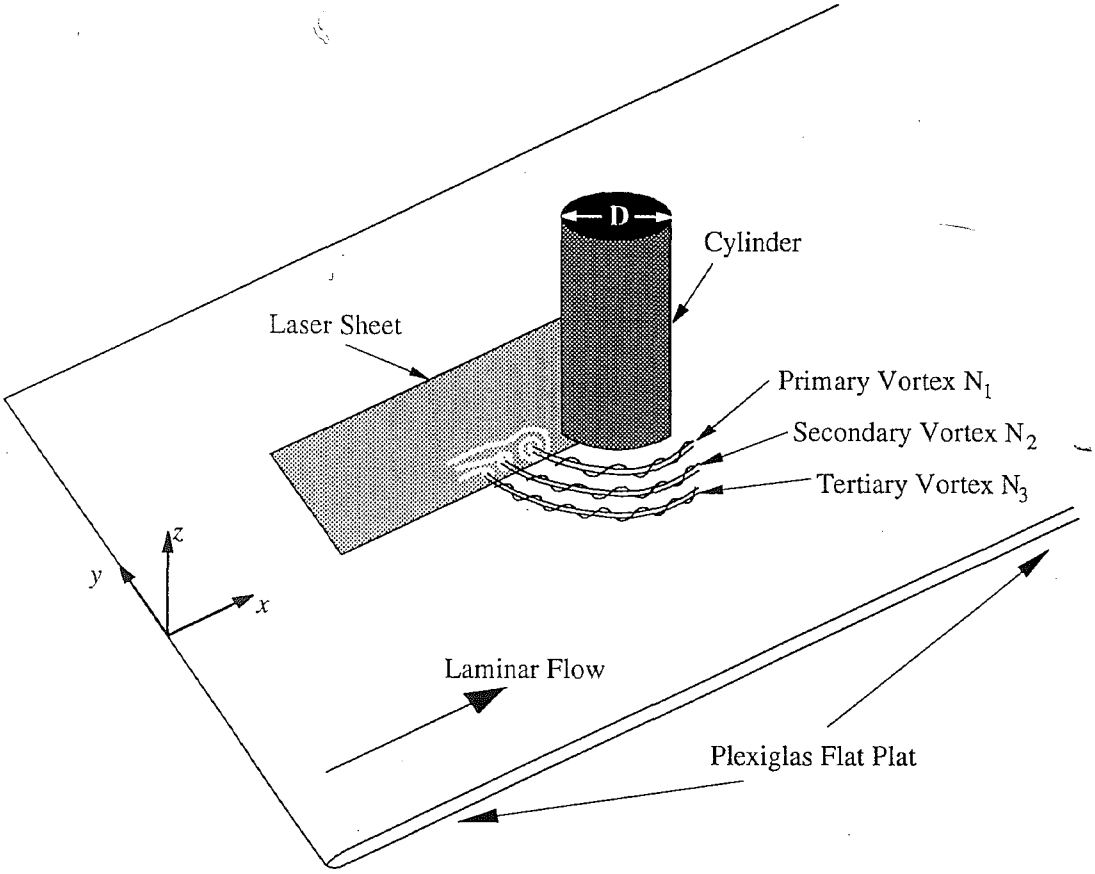

Figure 3.2 General Configuration of a Laminar, Steady Three-Vortex System

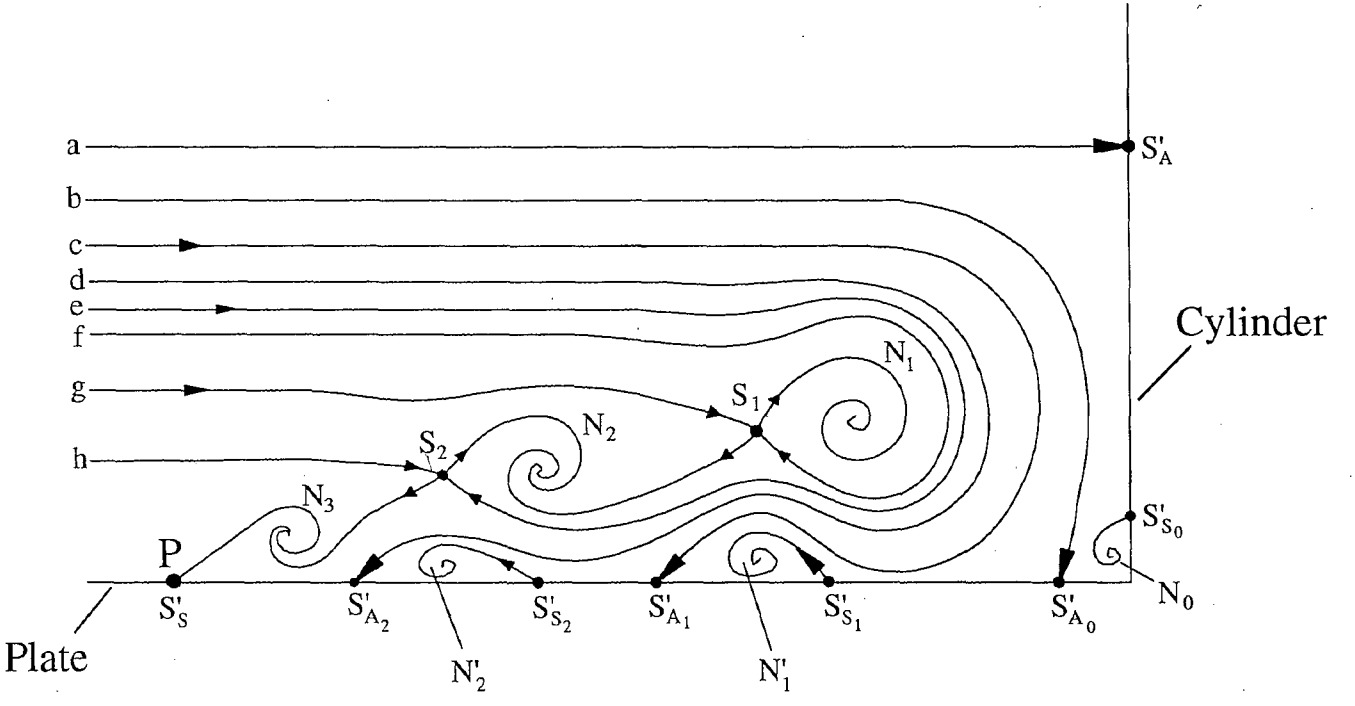

Figure 3.3 2-D Streamline Schematic of the Standard Jet-Maze Topology

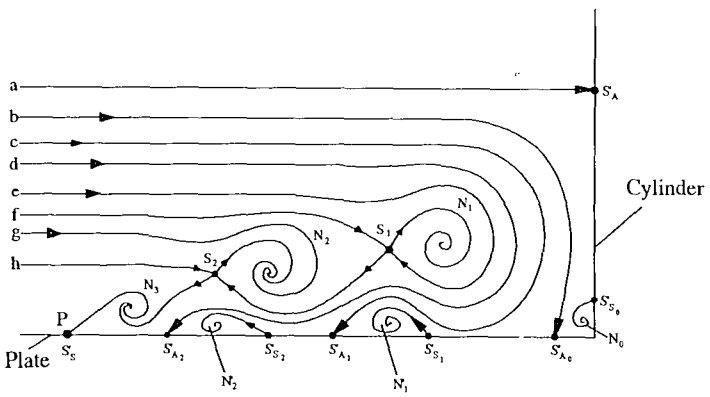

(a)

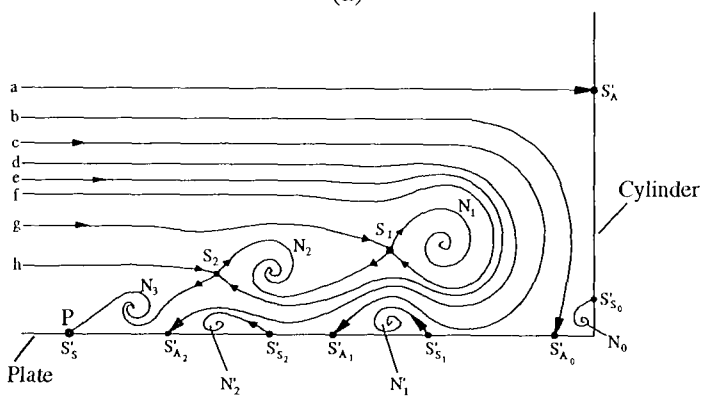

(b)

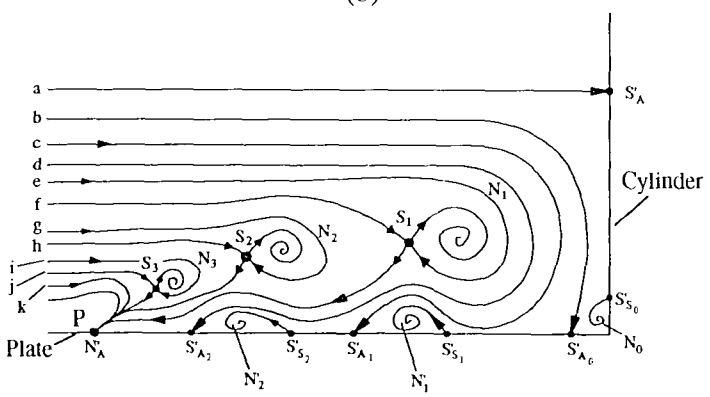

(c)

Figure 3.4 Steady, Laminar Three-Vortex Regimes
(a) Regime 1 Topology
(b) Regime 2 (Jet-Maze) Topology
(c) Regime 3 (Attachment) Topology

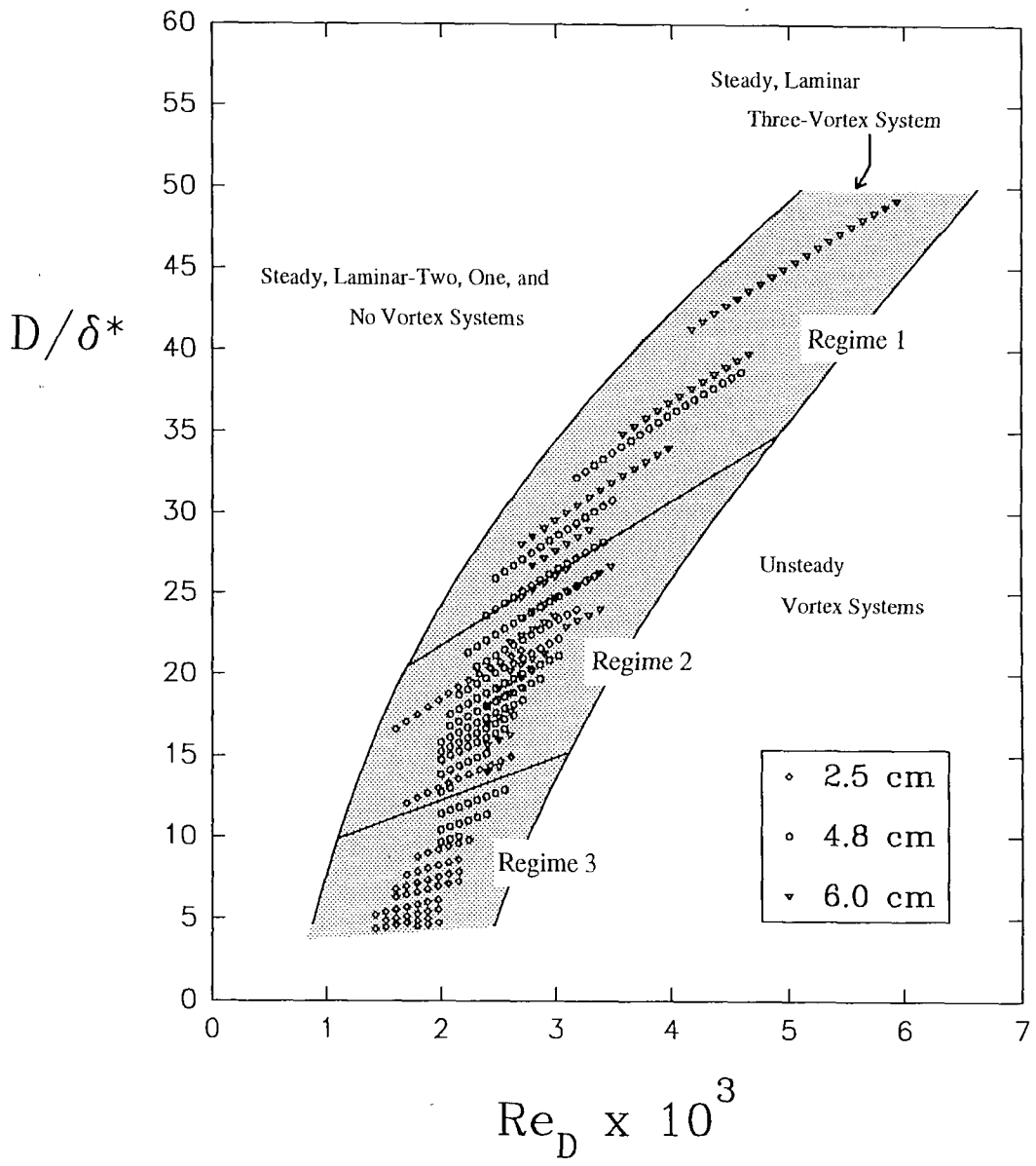

Figure 3.5 Parametric Locations of Three-Vortex Regimes Based on Re_D and D/δ^*

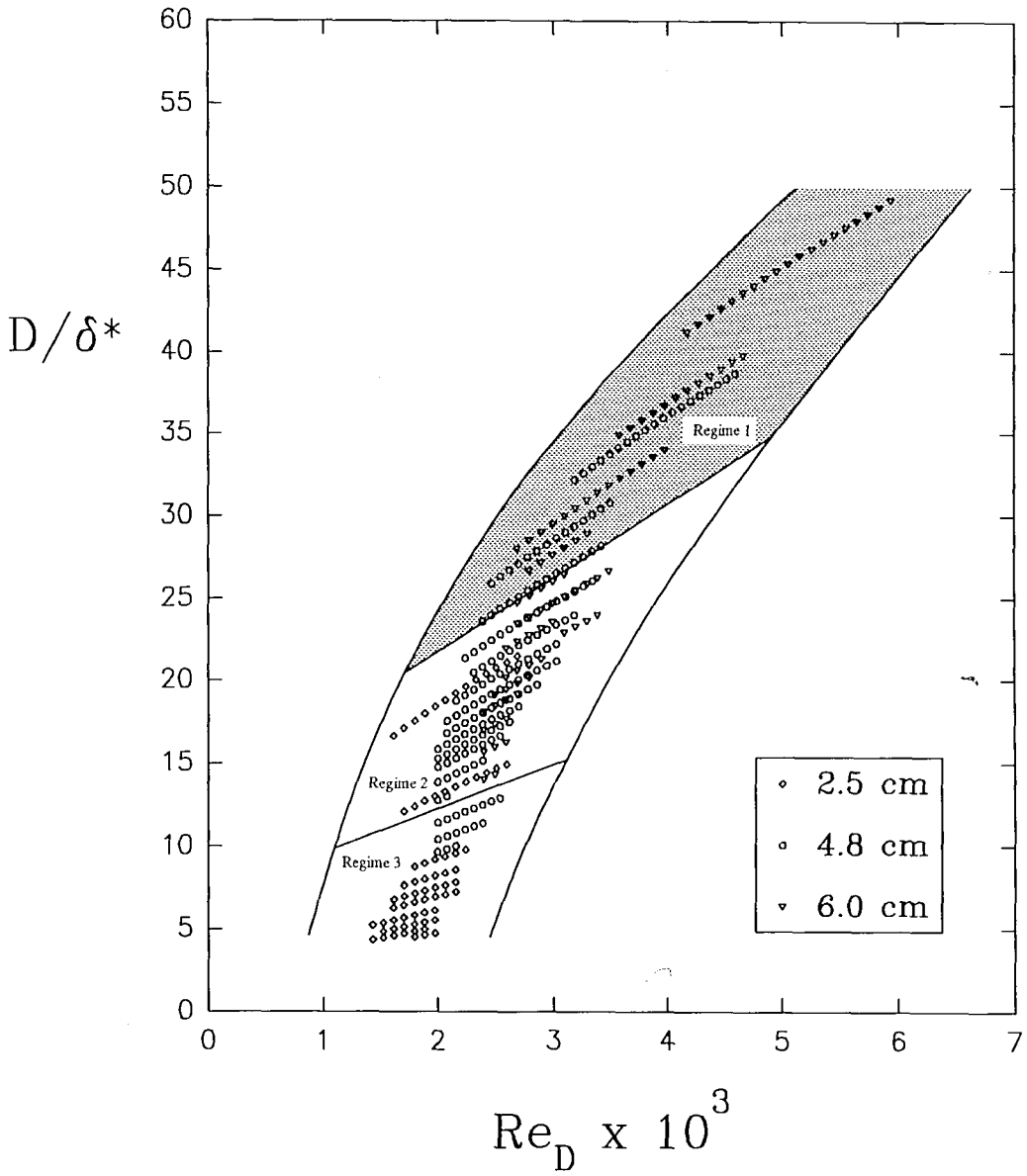

Figure 3.6 Region of Regime 1 Topology Based on Re_D and D/δ^*

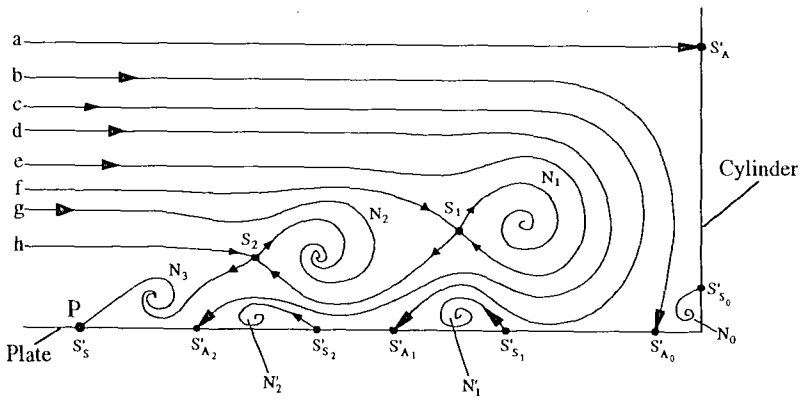

(a)

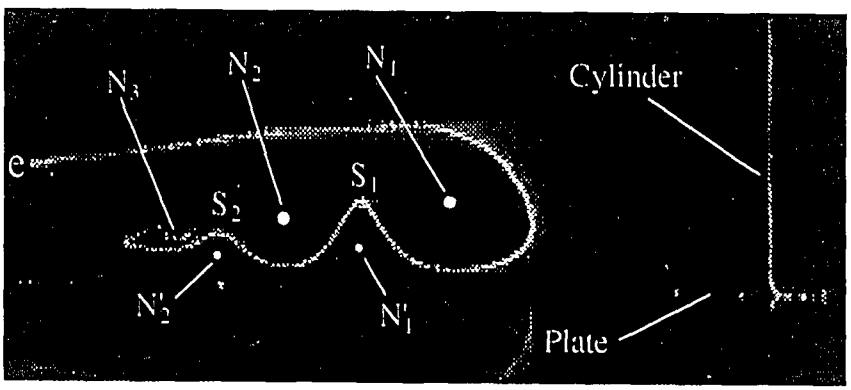

(b)

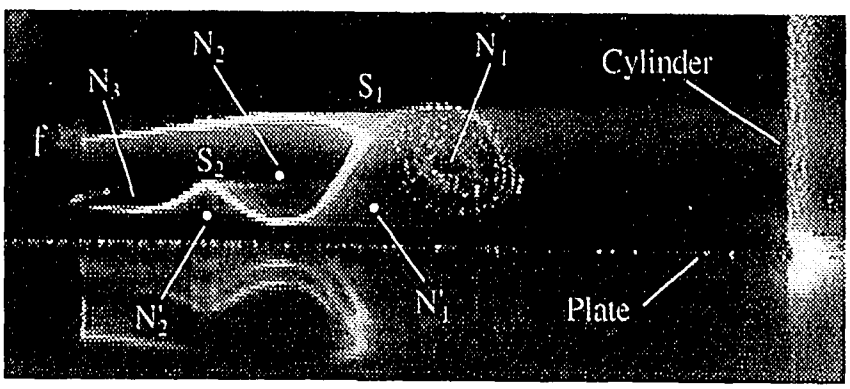

(c)

Figure 3.7 (a) 2-D Streamline Schematic of the Regime 1 Topology
(b) Hydrogen Bubble Visualization of Regime 1 (Feeding Streamline 'e')
(c) Hydrogen Bubble Visualization of Regime 1 (Feeding Streamline 'f')
($D/\delta^*=7$, $Re_D=1960$)

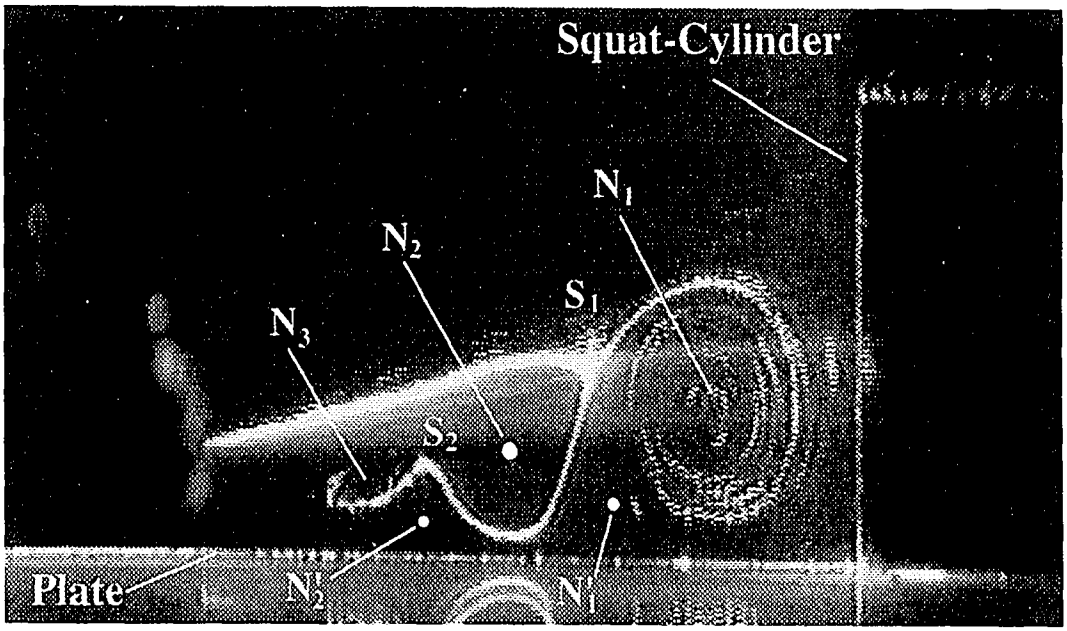

Figure 3.8 Hydrogen Bubble Visualization of the Regime 1 Topology Empolying a Squat-Cylinder ($h/D = 0.31$) For Flow Conditions $D/\delta^* = 32$ and $Re_D = 4000$.

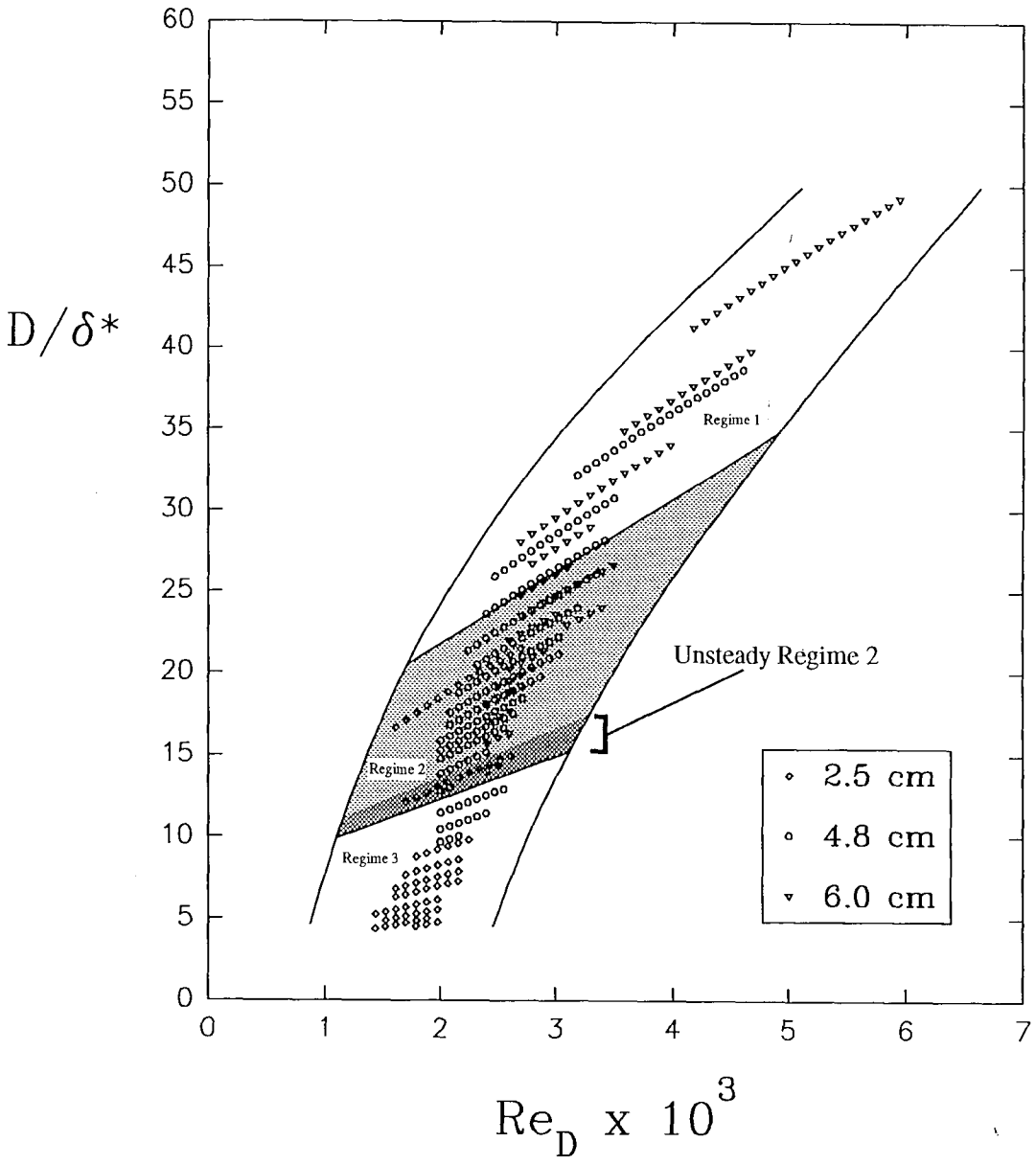

Figure 3.9 Region of Regime 2 Topology
Based on Re_D and D/δ^*

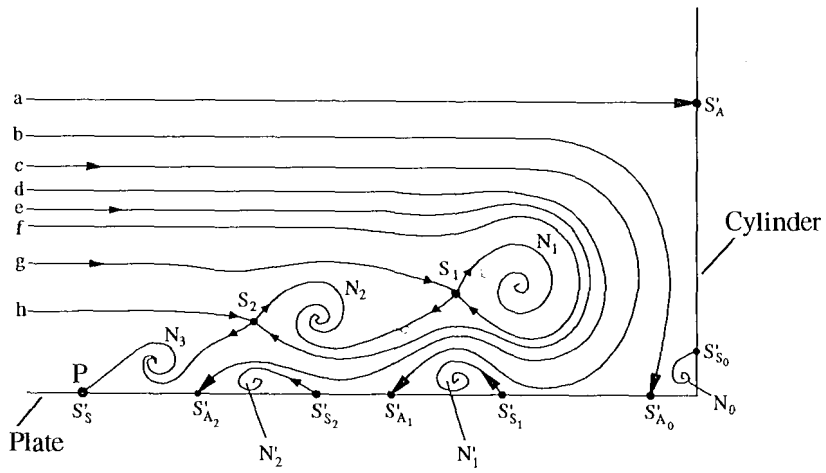

(a)

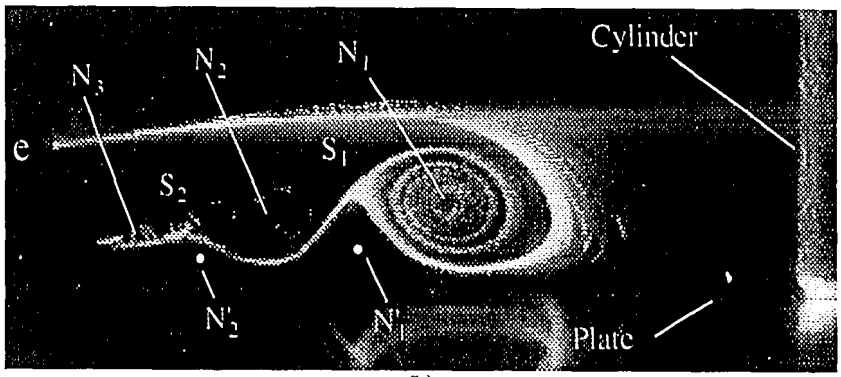

(b)

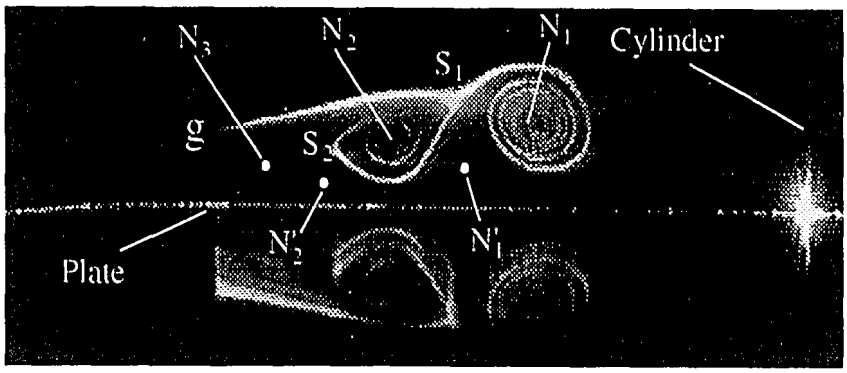

(c)

Figure 3.10 (a) 2-D Streamline Schematic of the Regime 2 (Jet-Maze) Topology
(b) Hydrogen Bubble Visualization of Regime 2 (Feeding Streamline 'e')
(c) Hydrogen Bubble Visualization of Regime 2 (Feeding Streamline 'g')
$\left(D/\delta^* = 18,\ Re_D = 2250\right)$

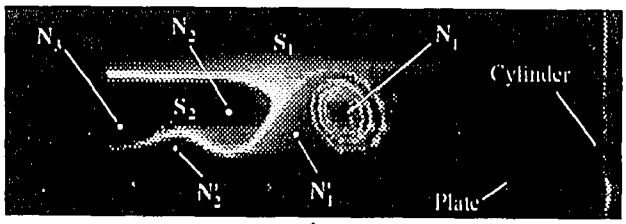

1

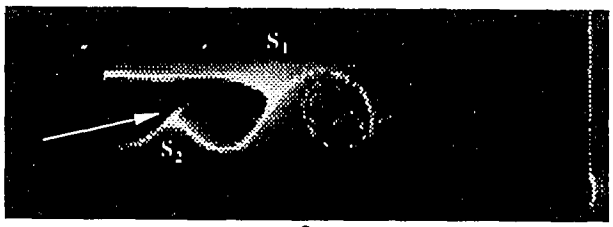

2

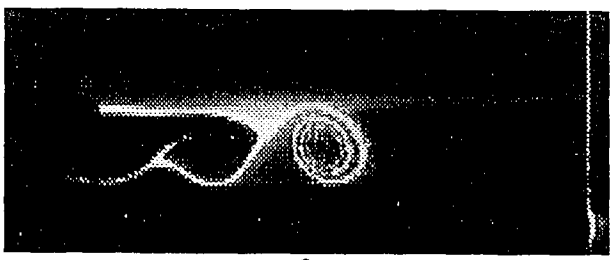

3

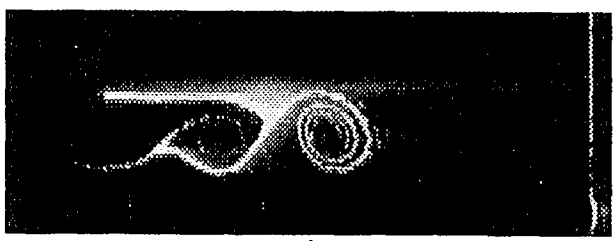

4

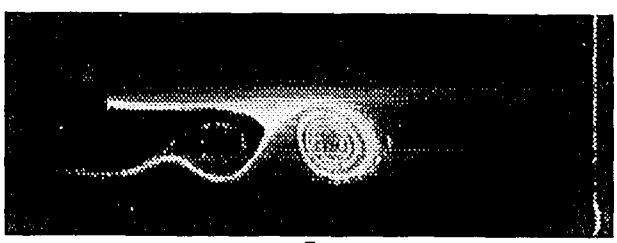

5

Figure 3.11 Unsteady Regime 2 Topology ($D/\delta^*=12$, $Re_D=1890$)

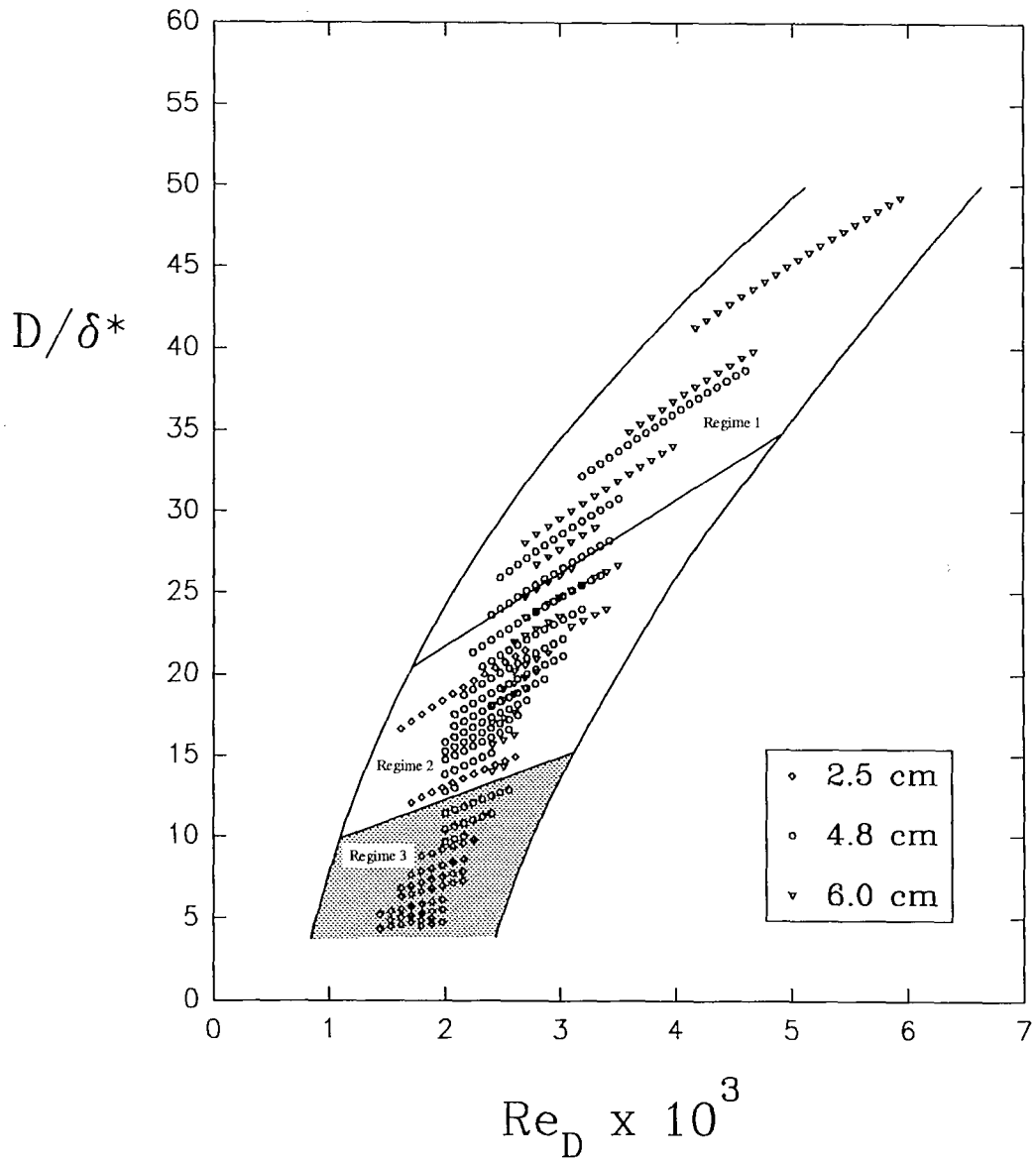

Figure 3.12 Region of Regime 3 Topology
Based on Re_D and D/δ^*

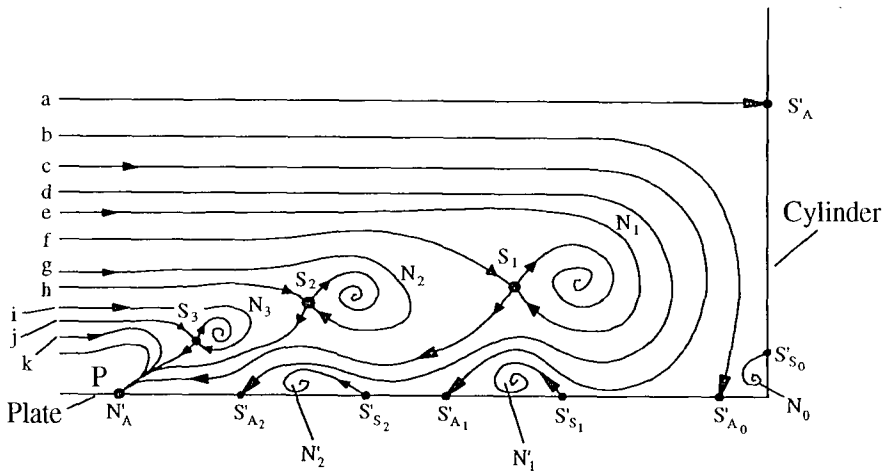

(a)

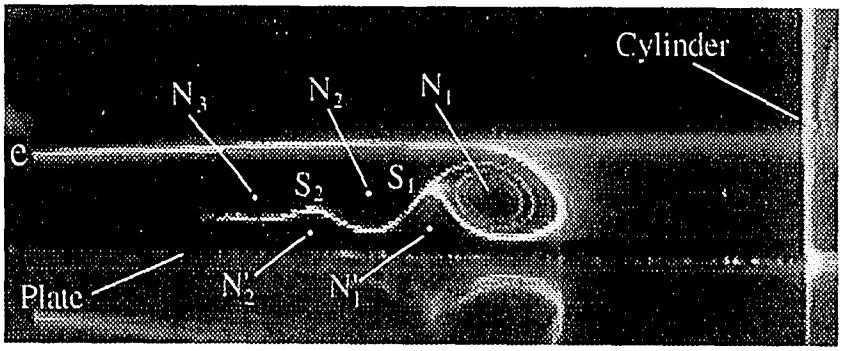

(b)

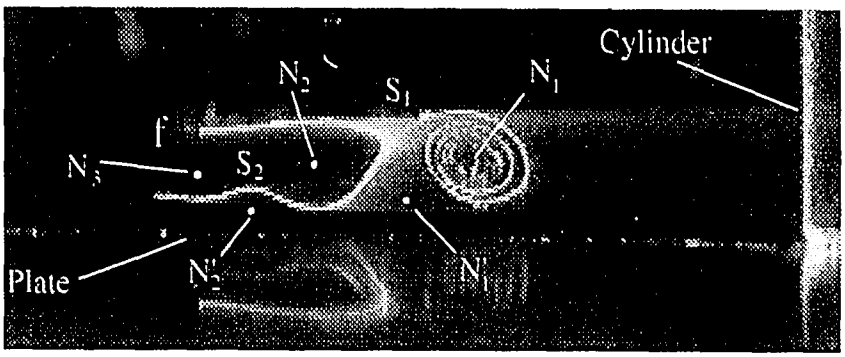

(c)

Figure 3.13 (a) Streamline Schematic of the Regime 3 Topology
(b) Hydrogen Bubble Visualization of Regime 3 (Feeding Streamline 'e')
(c) Hydrogen Bubble Visualization of Regime 3 (Feeding Streamline 'f')
($D/\delta^*=7$, $Re_D=1960$)

4.0 DISCUSSION OF RESULTS

4.1 Steady, Laminar Three-Vortex Regimes

4.1.1 General.

In this chapter, the Regime 1 and 3 topologies described in Chapter 3 will be compared and contrasted to both the standard Jet-Maze (Regime 2) topology and other previously suggested topologies. The present topologies will also be examined from the perspective of critical-point theory. Lastly, a discussion of the possible mechanisms which account for the development of the differing regime behavior will be presented.

4.1.2 Comparison of Regime 1 topology to the standard Jet-Maze (Regime 2) topology

In Chapter 3, the streamline 'feeding' characteristics of the Regime 1 topology were presented in detail as well as those of the standard Jet-Maze (Regime 2) topology, which in this study is designated as the Regime 2 topology. Both topologies are shown comparatively in Figure 4.1. The most significant difference between the Regime 1 topology and the Jet-Maze (Regime 2) topology lies in the connecting streamline behavior between the full saddle points S_1 and S_2. In Regime 1 (Figure 4.1a), streamline 'e' reflects off saddle point S_1 to saddle point S_2, subsequently reflecting off S_2 and feeding directly into the tertiary vortex N_3. This behavior can be directly compared to the standard Jet-Maze (Regime 2) topology shown in Figure 4.1b, where streamline 'f' reflects off saddle point S_1, but then feeds immediately into secondary vortex N_2, without reflecting off saddle point S_2.

Another significant difference between the Jet-Maze topology and the Regime 1 topology is the 'feeding' order of the main vortices. Starting at streamline 'd' in Figure 4.1a (Regime 1 topology) and traversing down through the boundary layer, note that the

tertiary vortex N_3 is first fed from the dark-gray layer 'd-e,' the primary vortex N_1 is fed next by the light gray layer 'e-f,' the secondary vortex N_2 is then fed by the medium-gray layer 'f-g-h,' and lastly the tertiary vortex N_3 is additionally fed by the shear layer between streamline 'h' and the plate as indicated by the dark-gray arrow. In contrast, for the Jet-Maze (Regime 2) topology the secondary vortex N_2 is 'fed' by two separate shear layers. As Figure 4.1b indicates, the secondary vortex N_2 is 'fed' by the light-gray layer 'e-f' and by layer 'g-h' respectively as one traverses down through the boundary layer. However, the Regime 1 topology and the Jet-Maze (Regime 2) topologies display identical 'feeding' streamlines for the tertiary vortex N_3, which is indicated in both Figure 4.1a and b by the dark-gray layers that feeds around primary vortex N_1 and by the dark-gray arrows. All of the remaining streamline feeding patterns are identical for the two topologies regarding the feeding of the counter-rotating vortices N_1', N_2', and N_0.

4.1.3 Comparison of Regime 3 (Attachment) topology to the standard Jet-Maze (Regime 2) topology.

As mentioned previously in Chapter 3, the Regime 3 (Attachment) topology is a new topology established computationally by Visbal (1990), and is associated with large boundary layer thicknesses and low Reynolds numbers. This topology is markedly different than other suggested topologies due to the presence of a half-nodal point of attachment (N_A') in lieu of the intuitive half-saddle point of separation (S_S') expected for these types of geometries and flow conditions. The Regime 3 (Attachment) topology additionally differs from the other topologies (Regimes 1 and 2) by the presence of a third full-saddle point (S_3) associated with the tertiary vortex N_3.

Figure 4.2 shows the comparative 'feeding' patterns of the Regime 3 (Attachment) topology and the standard Jet-Maze (Regime 2) topology. Recall that for the Jet-Maze (Regime 2) topology (Figure 4.2a), discussed in section 4.1.2, the main vortices are fed

in reverse order as one traverses down through the boundary layer; the tertiary vortex N_3 is fed first from the upper shear layer region 'd-e,' the secondary vortex N_2 is fed second by region 'e-f,' then primary vortex N_1 is fed last by region 'f-g.' By comparison, for the Regime 3 topology (Figure 4.2b), the order of 'feeding' of the main vortices is reversed, with the primary vortex N_1 fed first by the light-gray region 'e-f,' the secondary vortex N_2 fed by the medium-gray region 'g-h,' and the tertiary vortex N_3 is fed last by the dark-gray region 'i-j.'

4.2 Comparison with Prior Research Findings.

Most of the prior experimental, numerical and theoretical studies on juncture flows examined a broad range of behavior. For example, Norman (1972), Baker (1979, 1991), Sendey and Kitchens (1975), Schwind (1962), and Visbal (1991) studied a broad variety of juncture flow phenomena; in contrast, the present study focused singly on the steady, laminar three-vortex system at the cylinder/flat-plate juncture in order to understand the intricacies of the flow structure. The following compares and contrasts Regimes 1, 2 and 3 detemined in the present study, with the flow topology models suggested by previous studies.

4.2.1 Comparison of Regime 1 Topology

The Regime 1 topology of the present study is similar to the steady, laminar three-vortex topology hypothesized by Baker (1979), with one exception. Baker's topology (redrawn with nomenclature consistent with the present study) displays an unusual full-saddle point (S_1) to half-saddle point of attachment (S'_{A_2}) connection as shown in Figure 4.3b. For comparison, the Regime 1 topology is shown above Baker's topology in Figure 4.3a. In the Baker model, the primary vortex N_1 is fed first, vortex N_3

is fed second, and vortex N_2 is fed third; vortex N_3 is also fed from a shear layer near the surface, similar to Regime 1. Baker noted that his steady, laminar three-vortex topology was partly conjectured since he could not clearly tell which of vortices N_2 or N_3 was fed first as he brought his smoke probe closer to the surface. Clearly, Baker's model is similar to Regime 1, and is definitely not the standard Jet-Maze topology.

In Figure 4.4, Baker's parametric results indicating where he observed a steady, three-vortex system are superposed on the parametric results of the present investigation. Note that the Baker results indicate the steady, laminar three-vortex topology to persist for high values of Re_D and low values D/δ^*, in contrast to the present results. An examination of the parameter range of Baker was done in our facility, but the data at high Re_D and low D/δ^* indicated a departure from the steady, three-vortex system. Figure 4.5 shows a further comparison of the results of the present investigation with Greco's (1990) experimental data which indicate a similar trend to the present investigation's results. The suggestion is that Baker's parametric results may have been in error for low D/δ^* values, probably due to the influence of his visualization technique, as discussed earlier in Section 1.2.1.

4.2.2 Comparison of Regime 2 (Jet-Maze) Topology

As mentioned previously, the standard Jet-Maze (Regime 2) topology is hypothesized by many researchers as the only steady, laminar three-vortex topology for cylinder/flat-plate geometry. Norman (1972), Sedney et al. (1975) and Greco (1990) examined a number of different types of juncture flows, both laminar and turbulent, but reported no other steady, laminar three-vortex topologies in addition to Jet-Maze (Regime 2). However, Norman did observe a laminar, three-vortex topology he termed a 'Stairstep' topology, but could observe no clearly steady case. The Stairstep topology,

shown originally in Figure 1.2, which is redrawn in critical point nomenclature in Figure 4.6b, displays two unusual full-saddle point to half-saddle point of attachment connections $\left(S_1 \rightarrow S'_{A_1} \text{ and } S_2 \rightarrow S'_{A_2}\right)$, in comparison to the Jet-Maze (Regime 2) topology shown in Figure 4.6a. However, Baker's topology, shown in Figure 4.6c, while topologically different, does display this unusual type of connection $\left(S_1 \rightarrow S'_{A_2}\right)$ as well. This type of critical point connection is considered unusual for it is very rare to have to saddle points connected to one another. While topologically possible, neither the Stairstep nor the Baker topology correspond to any of the topologies of the present study. Note that both Baker and Norman employed smoke sheet generation in their respective wind tunnel studies to examine the streamline feeding behavior of the steady, laminar three-vortex system. Norman, in addition to smoke sheet generation for streamline feeding, injected smoke from the endwall to visualize both the counter-rotating vortices N'_1, N'_2, as well as the flow behavior to and from the outermost saddle-point of separation S'_S. The present study suggests that flow disturbances caused by both these types of flow visualization methods could easily cause the breakdown of any topology under investigation to the Regime 2 (Jet-Maze) topology, thus leading to erroneous conclusions. The disturbance caused by his visualization technique are the most likely reason that Norman could find no clear steady case of the Stairstep topology, which seems to be a hybrid of the Regime 2 and Regime 3 topologies. Additionally, many researchers including Baker (1979, 1991), Greco (1990), Norman(1972) and Schwind (1962) have attempted to explain oscillations of multiple vortex systems. The present results suggest that at least some of the system oscillations noted by the above researchers could have been due to the intermittent switching of the outermost critical point between a half-saddle point of separation and half-nodal point of attachment.

Using a full Navier-Stokes computation of a laminar cylinder-juncture flow, Visbal (1991) identified two distinct steady, laminar three-vortex topologies for two different sets of flow parameters (Figure 1.7): the standard Jet-Maze (Regime 2) topology, and a new type, which the present paper will refer to as the Regime 3 (Attachment) topology. A computation performed by Visbal for $Re_D = 3500$ with a flat plate leading edge located at $x/D = -2.0$ and $h/D = 2.0$ (where h corresponds to the height of the cylinder measured from the flat-plate surface) indicated the presence of a Regime 2 (Jet-Maze) topology ($\beta_p > 1$). This data point is plotted in comparison with the data from the present study on Figure 4.7. Visbal's test location $\left(x/D = -2.0 \Rightarrow D/\delta^* = 22\right)$ falls in the middle of the parameter space occupied by the Regime 2 (Jet-Maze) topology, but lies just outside the bounding curve between the steady, laminar three-vortex parameter region and the unsteady vortex parameter region. Even though Visbal's test location data point lies just outside the steady, laminar three-vortex region, it falls well within the range of D/δ^* for which the Regime 2 (Jet-Maze) topology exists, thus indicating very good agreement between the present experimental and Visbal's computational results.

Perry et al. (1974) and Perry et al. (1987) applied critical point theory to classify the many types of critical points that exist in both laminar and turbulent flows. In addition to the classification of critical points, Perry et al. (1987) discuss the structural stability of flows containing critical points. Displaying the critical points on a p-q chart (Figure 4.8), where p and q represent the eigenvalue solution vectors to the Navier-Stokes and continuity equations, one can classify a critical point as either a node, foci or saddle. If the eigenvalues are real, either nodes or saddles can be produced, as in the case of the steady, laminar three-vortex system, and the pattern of flow in the vicinity of the critical point (node, foci or saddle) depends on the region of the p-q chart that point falls

within. Perry et al. (1987) state that if a critical point is infinitesimally close to the p axis of the p-q chart, then an infinitesimal change in any of the relevant parameters (i.e. the derivatives of the vorticity field), could result in a switch from a saddle to node, or vice versa, thus causing a change in the topological structure. This is essentially the case when the Regime 2 (Jet-Maze) topology begins to switch to a Regime 3 (Attachment) topology as illustrated in Figure 3.11; the sensitivity of this region on the p-q chart results in the irregular fluctuation of the steady, laminar three-vortex system. During this transition, the outermost separation point (S'_S), a saddle point, switches to an attachment point (N'_A), a node. The driving force of this switching process is the vorticity ratio parameter β_P proposed by Visbal (1990), which is equivalent to the η_x/ξ_y parameter defined by Perry et al. (1974), which ultimately governs whether the flow is separating or attaching at the outermost critical point P.

4.2.3 Comparison of Regime 3 (Attachment) Topology

Visbal (1991) first identified the Regime 3 (Attachment) topology, in a computational study for the flow conditions $Re_D = 2600$ and $\delta_o/D = 0.1$, where δ_o is the boundary layer thickness. Visbal's data point for this flow condition is also plotted in comparison with the parametric results of the present study in Figure 4.7. Performing the appropriate conversion calculations, note that Visbal's test location $\left(\delta_o/D = 0.1 \Rightarrow D/\delta^* = 6.5 \text{ and } Re_D = 2600\right)$ corresponds roughly to the lower range of the present study and is slightly into the parameter range defining unsteady vortex regimes. As mentioned previously, the type of flow topology near the outermost coalescence point P is determined by the value of the separation parameter $\beta_P = \left(\partial\omega_y/\partial x\right)/\left(\partial\omega_x/\partial y\right)$ where ω_x and ω_y denote the vorticity components in the x and y directions respectively. For $\beta_P > 1$, P is a separation point (Regime 2/Jet-Maze

topology), while for $\beta_P < 1$, P is a point of attachment (Regime 3/Attachment topology). For his computational Regime 3 (Attachment) topology, Visbal calculated the $\beta_P = 0.93$, which is consistent with the aforementioned criteria first presented by Perry et al (1987) for the outermost convergence line (point P) to be one of attachment.

In that same year, Hung et al. (1991) confirmed Visbal's Attachment (Regime 3) topology in a separate computational study for the flow conditions $M_\infty = 2.0$ and $Re_D = 1500$. In their study, Hung et al. allowed the boundary layer thickness to grow, according to $\delta = 5.0x/Re_x^{1/2}$, from an initial boundary layer thickness parameter δ_o/D = 0.1 initiated 10D upstream of the cylinder. Performing the appropriate conversion calculations, the parametric location of Hung et al.'s attachment topology $(D/\delta^* = 6.8$ and $Re_D = 1500)$ corresponds very well with the present study's data, falling well within the parameter space for the Regime 3 topology, as shown in Figure 4.7. The results of Visbal and Hung et al. indicate that at least two different types of steady, laminar three-vortex topologies are possible, and the actual type of topology which will prevail in a given case is a function of β_P. The results of the present study provide insight to the dependence of this parameter on Re_D and D/δ^*.

The Stairstep topology proposed by Norman (1972) could have been some variation of the Regime 3 topology since the feeding characteristics of the main vortices (N_1, N_2, N_3) are identical. As mentioned previously, Norman could find no clear steady case of the Stairstep topology, most likely due to the disruptive effects of the smoke flow visualization method he employed. Comparing the 2-D streamline schematics of the Regime 3 topology and the Stairstep topology in Figure 4.9, there are a number of differences. Note the Stairstep's connection of the full-saddle points S_1 and S_2 to the flat-plate surface half-saddle points of attachment S'_{A_1} and S'_{A_2}, respectively. For the Regime 3 (Attachment) topology, there are no such connections. Recall that Baker's model also

displayed a similar behavior in the connection of a full-saddle point S_1 to a half-saddle point of attachment S'_{A_2}. None of these unusual characteristics were observed by the present author in any of the topological Regimes presented in this study. The last and most significant difference between the two topologies is that the outermost point P is a point of separation for the Stairstep topology, but is one of attachment for the Regime 3 (Attachment) topology. Considering the sensitivity of the various topologies noted in the present study, it would seem that the differences in the model topologies of Norman and Baker from the present topologies are due to their method of smoke introduction, and their capability for closely interpreting their resultant patterns.

4.3 Critical-Point Analysis of the Regimes.

Examining the kinematics of streamline patterns in laminar flows around three-dimensional surface obstacles, Hunt, et al. (1978) derived certain topological constraints for flow, laminar or turbulent, near the critical points. For two-dimensional plane sections of the flow, the critical points are constrained by the relation:

$$\left(\sum N+\frac{1}{2}\sum N'\right)-\left(\sum S+\frac{1}{2}\sum S'\right)=1-n, \qquad (4.1)$$

where n is the connectivity of the section of the flow considered and N, N′, S and S′ are the critical points located along the surface upstream of the juncture. Referring to the 2-D streamline schematic of the Regime 1 topology in Figure 4.1(a), and assigning the appropriate number of critical points in (4.1):

$$\sum N=4, \quad \sum S=2, \quad \sum N'=2, \quad \sum S'=6$$

so that

$$\left(\sum N+\frac{1}{2}\sum N'\right)-\left(\sum S+\frac{1}{2}\sum S'\right)=(4+1)-(2+3)=0$$

The Regime 1 topology is in agreement with (4.1) since the cylinder/flat-plate juncture region under investigation is singly connected, so that $n = 1^*$. In fact, the Regime 2 (Jet-Maze), the Baker, and Norman's Stairstep topology are all in agreement with (4.1), since each display identical numbers of cumulative critical points both above and on the flat-plate (Figure 4.6a, b & c). Each topology differs only in the streamline pattern in and around these critical points. Since there is exact agreement with (4.1), the Regime 1 topology, as well as all the other topologies mentioned above, all are "kinematically" possible (i.e. each topology is compatible with a continuous and finite mean or instantaneous velocity field).

The agreement with (4.1) for all the topologies mentioned above is actually intuitive, since the skin-friction portrait for each is identical. That is, the number and sequence of critical points along and above the plate (Figures 4.6a, b & c) are identical. For example, the only difference between the Regime 1 and Regime 2 topologies is the manner in which streamlines 'feed' the main vortices. Figure 4.10 shows a plan-view of the skin-friction portrait created by both topologies. In Figure 4.10, arrows indicate the limiting streamlines (streamlines immediately adjacent to the surface) as well as three lines of convergence (denoted as lc_1, lc_2, lc_3) and lines of divergence (ld_1, ld_2, ld_3) consistent with the steady, laminar three-vortex topology (Regime 1 and Regime 2). These lines of convergence and divergence are lines of separation and attachment, respectively. Note once again, that since the Regime 1, Regime 2, Stairstep, and Baker topology exhibit identical skin-friction patterns on a flat-plate surface, this illustrates that surface optical-tracer techniques, such as powder suspensions in oil (Hunt et al. 1978,

* For example, if a hole were present through the base of the cylinder in the streamwise direction, similar to a causeway beneath a building, the region would be considered doubly connected.

Sedney et al. 1975) will not allow one to physically infer the details of the topological structure (i.e. the 'feeding' streamlines) above the plate.

Applying (4.1) to the Regime 3 (Attachment) topology, and keeping in mind that this topology has an additional full-saddle point S_3 and that the outermost point P is now a half-nodal point of attachment, we obtain:

$$\sum N = 4, \quad \sum S = 3, \quad \sum N' = 3, \quad \sum S' = 5$$

$$\left(\sum N + \frac{1}{2}\sum N'\right) - \left(\sum S + \frac{1}{2}\sum S'\right) = (4+1.5) - (3+2.5) = 0,$$

which again satisfies the topological constraints proposed by Hunt et al. (1978). Note that the skin-friction pattern of the Regime 3 (Attachment) topology is equivalent to that for Regime 1 and 2 topologies (Figure 4.10), which once again reinforces the limitations of optical-surface visualization methods. Using optical-surface visualization methods, researchers note the presence of 'accumulation' lines, usually consisting of powder suspensions in oil coated on the flat-plate surface surrounding the juncture. As Figures 1.5a and c show, the streamlines immediately adjacent to the flat-plate surface (limiting streamlines), move towards $(\pm x)$or away $(\pm y)$ from the separation/attachment point 0 in equivalent directions, thus displaying identical skin-friction patterns or skin-friction portraits (Figure 4.10). Obviously the flow in and around the separation or attachment point would induce identical 'accumulation' lines on the flat-plate surface, giving no indication whatsoever of the streamline pattern or the three-dimensional topological flow structure above the surface.

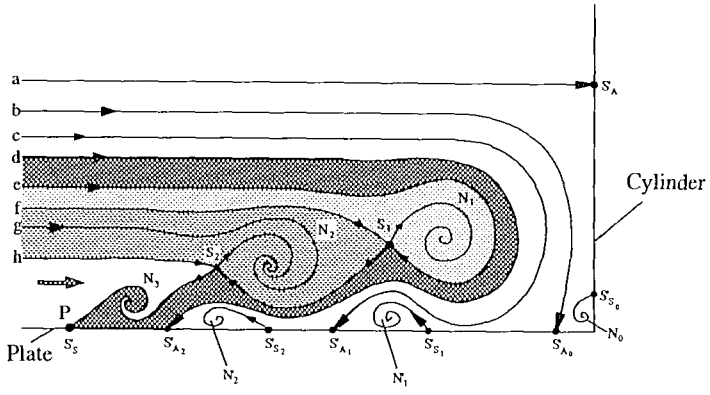

(a)

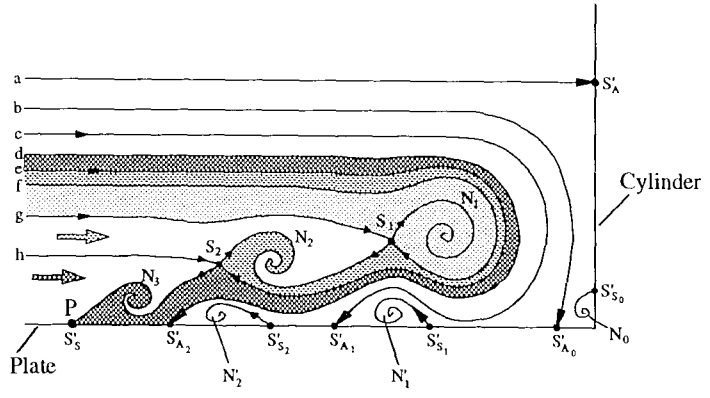

(b)

Figure 4.1 Comparative "Feeding" Patterns of Regime 1 and Regime 2 topologies
(a) Regime 1 Topology
(b) Regime 2 (Jet-Maze) Topology

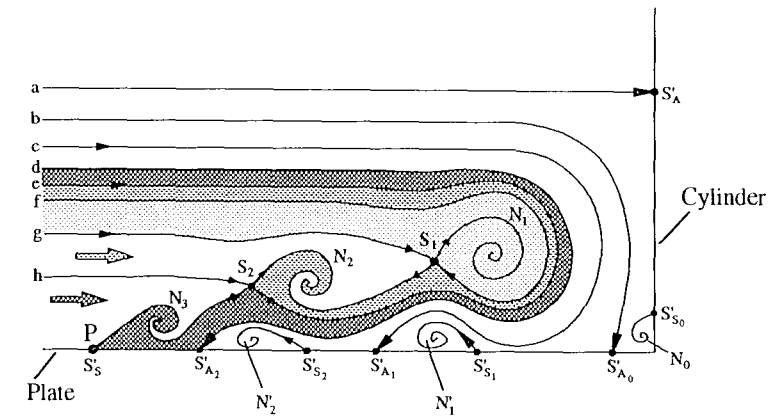

(a)

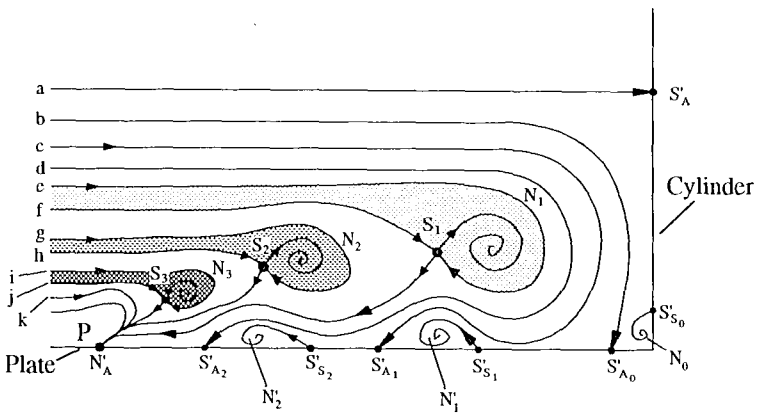

(b)

Figure 4.2 Comparative "Feeding" Patterns of Regime 2 and Regime 3 topologies
(a) Regime 2 (Jet-Maze) Topology
(b) Regime 3 (Attachment) Topology

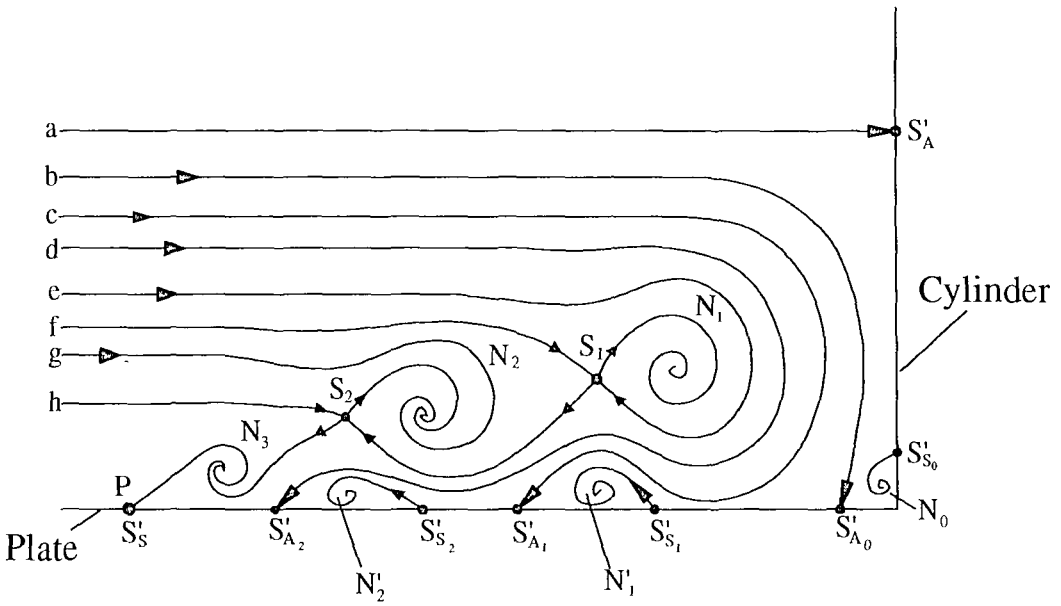

(a)

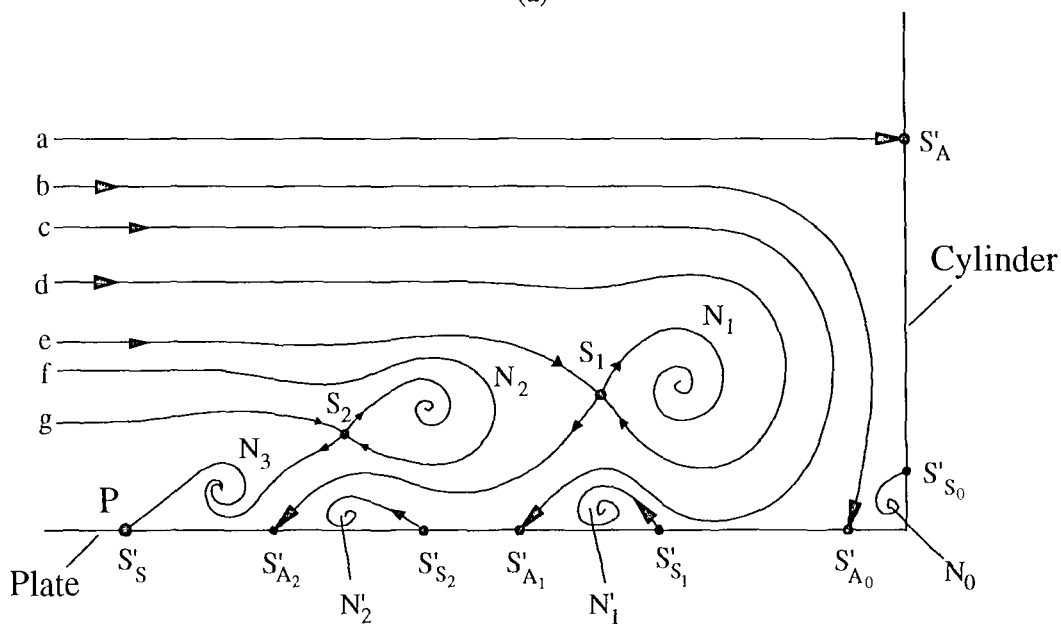

(b)

Figure 4.3 Comparison of Regime 1 with the Baker Topology
(a) Regime 1 Topology
(b) Baker Topology

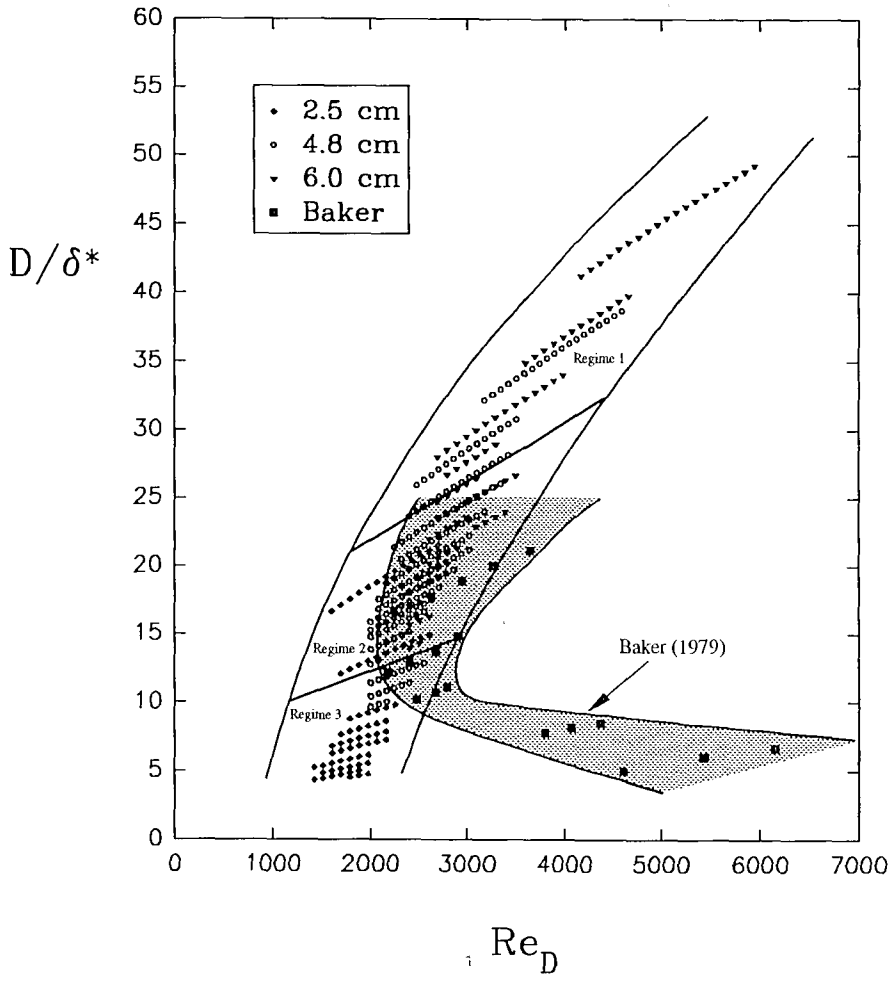

Figure 4.4 Comparison Plot of Three-Vortex Regime Data of Baker (1979) with Regime Data of Present Study

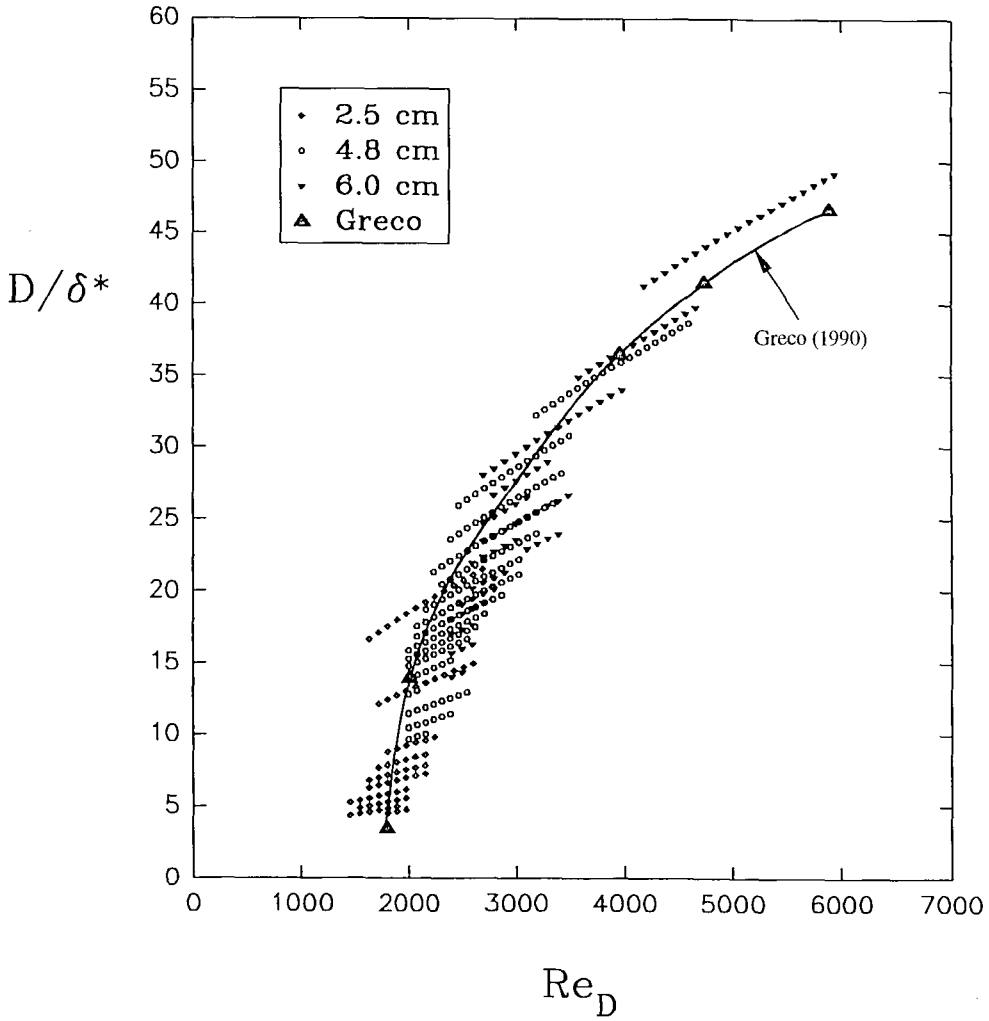

Figure 4.5 Comparison Plot of Three-Vortex Regime Data of Greco (1990) with Regime Data of Present Study

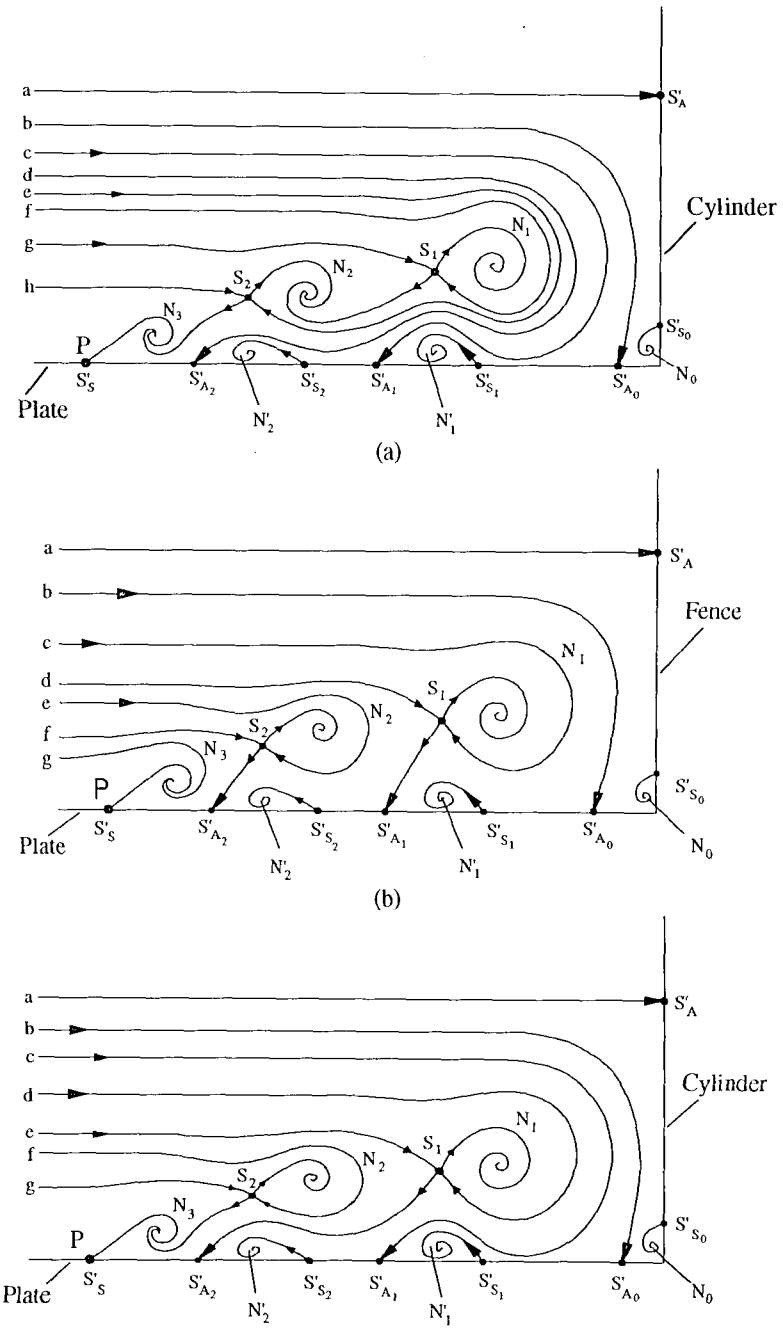

Figure 4.6 Comparison of Regime 2 Topology with the Stairstep and Baker Topologies
(a) Regime 2 (Jet-Maze) Topology
(b) Stairstep Topology (Norman, 1972)
(c) Baker Topology

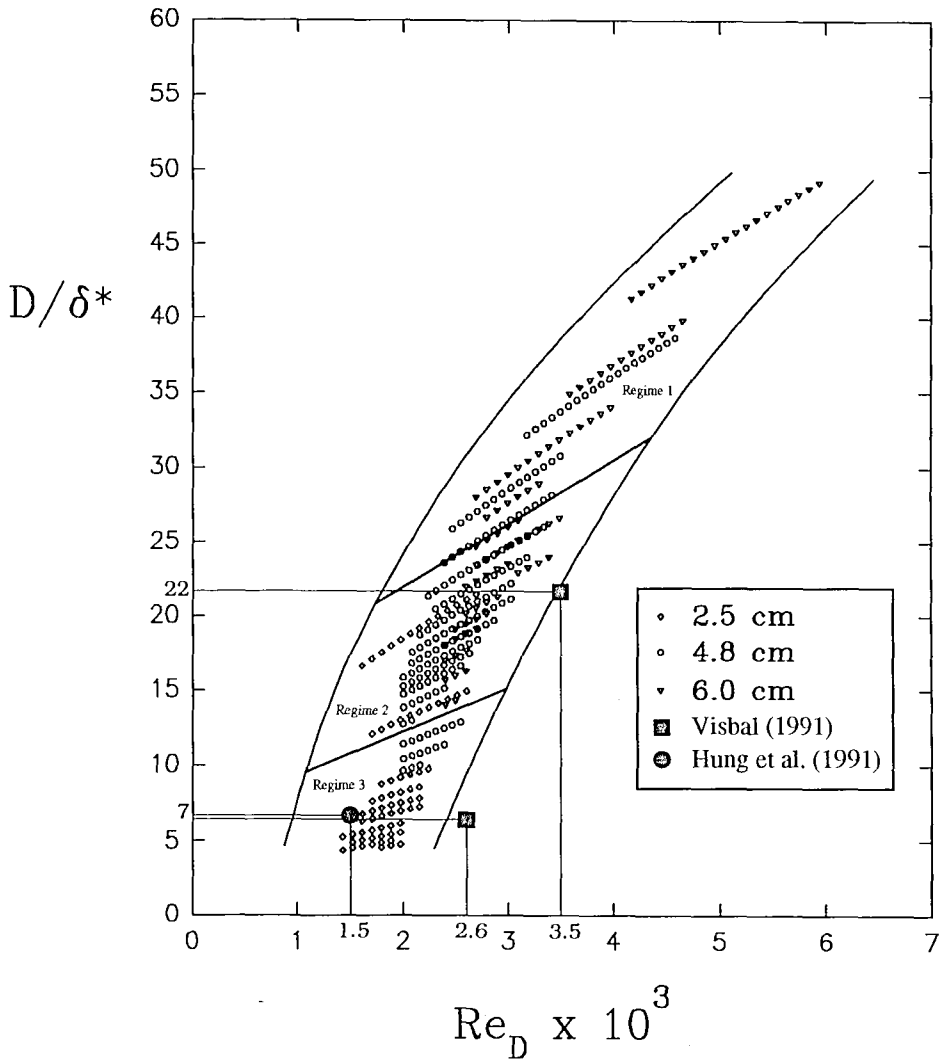

Figure 4.7 Comparison Plot of Three-Vortex Regime Data of Visbal (1991) and Hung et al. (1991) with Regime Data of Present Study

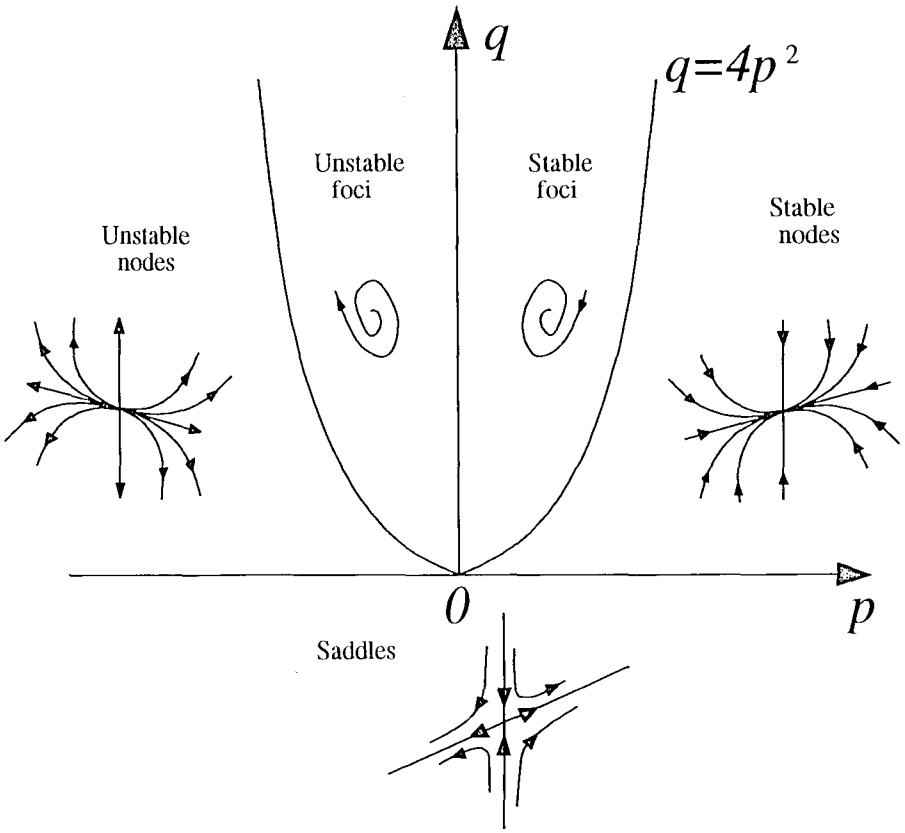

Figure 4.8 The *p-q* chart classification of critical points

(Perry and Fairlie, 1974)

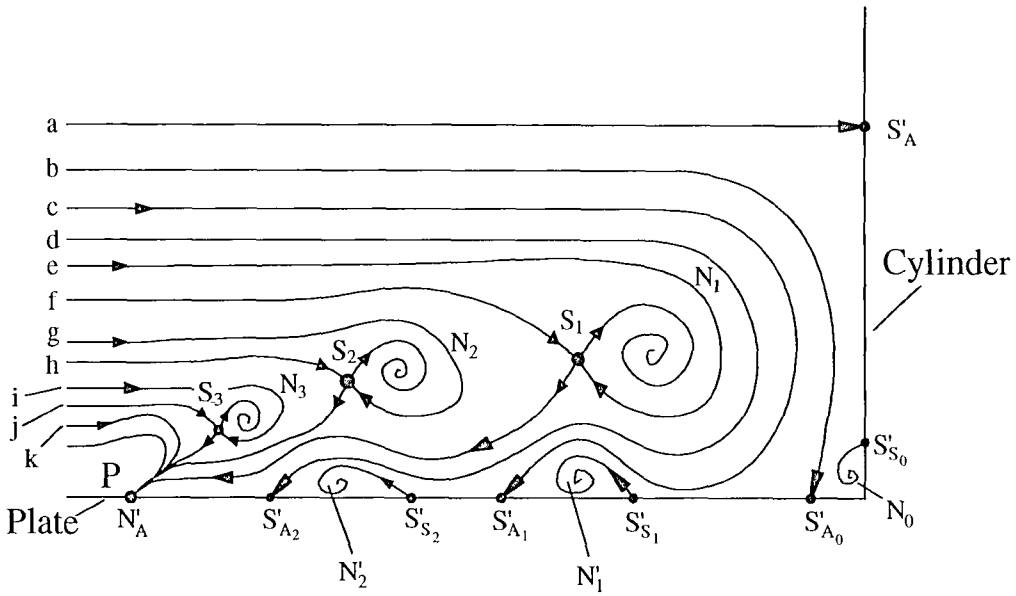

(a)

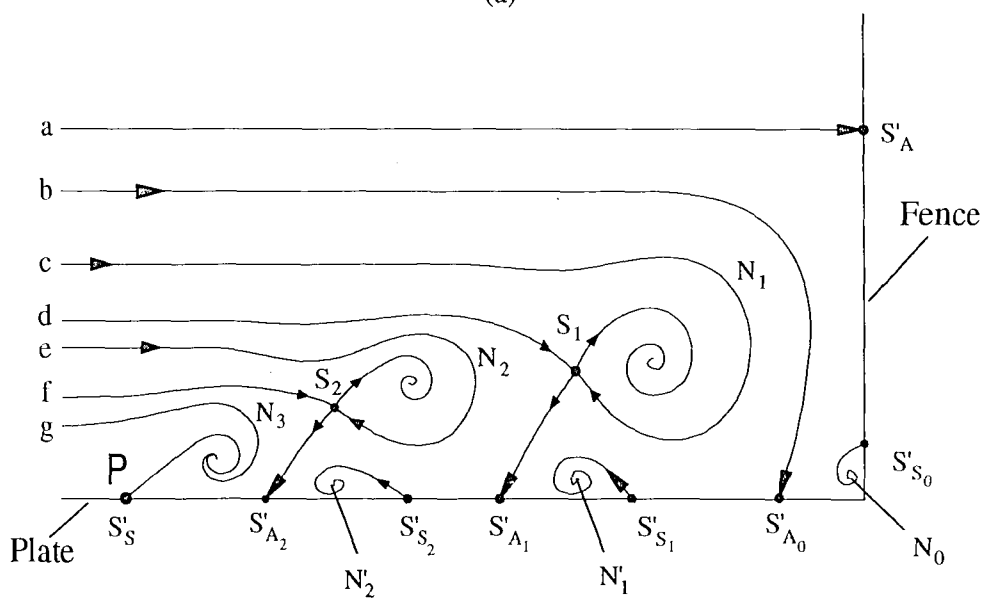

(b)

Figure 4.9 Comparison of Regime 3 Topology with the Stairstep Topology
(a) Regime 3 (Attachment) Topology
(b) Stairstep Topology (Norman, 1972)

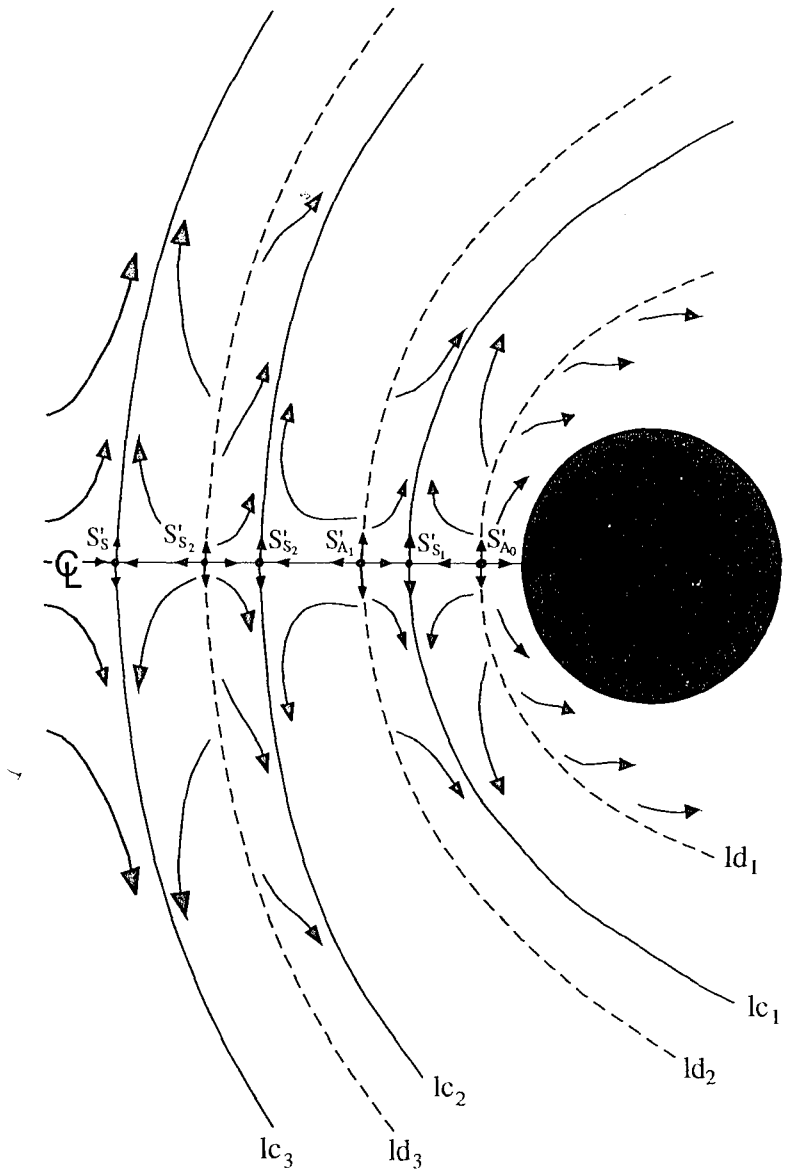

Figure 4.10 Skin-friction lines for all steady, laminar three-vortex topologies

5.0 SUMMARY AND CONCLUSIONS

The present experimental study documents the characteristics of three distinct steady, laminar three-vortex flow regimes in the boundary layer region near a flat plate-cylinder juncture. For certain ranges of Reynolds number, and dependent on the particular flow geometry, a steady, three-vortex system forms about the base of a cylinder and is the dominant flow structure of the region. The flow passes through a series of three distinct flow regimes which are clear functions of Reynolds number and boundary layer thickness. These regimes are: (a) a new type of separation point topology (Regime 1) which has not been previously detected, (b) the standard Jet-Maze separation point topology (Regime 2), and (c) a new 'attachment' point topology (Regime 3) proposed by Visbal (1991). The observed details of these steady, laminar flow regimes are documented in detail Chapter 3.

Based on the results of this study, in can be concluded that:

- At least three distinct steady, laminar three-vortex topologies exist, two separation types, one of which was previously undetected, and one attachment type; each topology occupies a specific parameter space based on Re_D and D/δ^*.

- The transition from one regime to the next occurs quite discretely; at the regime boundaries, small changes in the controlling parameters result in a complete modification of the topological structure, and thus the manner in which vorticity is fed into the main vortices.

- At the transition boundary between Regime 2 and 3, a narrow region exists within which the regime fluctuates randomly between the two adjacent topological structures, with the outermost separation line switching between one of separation and one of attachment.

REFERENCES

Baker, C.J., "The Laminar Horseshoe Vortex," J. Fluid Mech., Vol. 95, part 2, pp. 347-367.

Baker, C.J., "The Oscillation of Horseshoe Vortex Systems," J. Fluids Engng., Vol. 113, (1991), pp. 347-367, September 1991.

Clutter, D. W., Smith, A. M. O., "Flow Visualization by Electrolysis of Water," Aerospace Engineering, pp. 24-27 & 74, Vol. 20, January 1961

Greco, J., "The Flow Structure in the Vicinity of a Cylinder-Flat Plate Junction: Flow Regimes, Periodicity, and Vortex Interactions," M.S. Thesis, Dept. of Mechanical Engineering and Mechanics, Lehigh University, December 1990.

Hung, C.M, Sung, C.H. & Chen, C.L., "Computation of Saddle Point of Attachment," AIAA paper No. 91-1713, June 1991.

Hunt, J.C.R., Abell, C.J., Peterka, J.A. & Woo, H., "Kinematical Studies of the Flows Around Free or Surface-Mounted Obstacles; Applying Topology to Flow Visualization," J. Fluid Mech., Vol 86, part 1, pp. 179 -200.

Metzler, S.P., "Processes in the Wall Region of a Turbulent Boundary Layer," M.S. Thesis, Dept. of Mechanical Engineering and Mechanics, Lehigh University, 1980

Norman, R.S., "On Obstacle Generated Secondary Flows in Laminar Boundary Layers and Transition to Turbulence," Ph.D. Thesis, Illinois Institute of Technology. December 1972.

Panton, R.L., Incompressible Flow, John Wiley & Sons, Inc., New York, New York, 1984

Perry, A.E. & Chong, M.S., "A Series-Expansion Study of the Navier-Stokes Equations for Three-Dimensional Flow Separation Patterns," J. Fluid Mech., Vol. 173, pp. 207-223, December 1986.

Perry, A.E. & Fairlie, B.W., "Critical Points in Flow Patterns," Advances in Geophysics, Vol. 18B, pp. 299-315, 1974.

Schraub, F. A., Kline, S. J., Henry, J., Runstadler, P. W., Littel, A., "Use of Hydrogen Bubbles for Quantitative Determination of Time-Dependent Velocity Fields in Low-Speed Water Flows," Transactions of A.S.M.E., J. of Basic Engng., pp. 429-444, Vol. 87, June 1965

Schwind, R. G., "The Three-Dimensional Boundary Layer Near a Strut," Gas Turbine Lab. Report Number 67, M.I.T., May 1962

Sedney, R. & Kitchens, C.W. Jr., "The Structure of Three-Dimensional Separated Flows in Obstacle, Boundary-Layer Interactions," AGARD-CP-168, May 1975.

Taylor, B.K., "Pressure Gradient Effects on the Development of Hairpin Vortices in an Initially Laminar Boundary Layer," Ph.D. Thesis, Dept. of Mechanical Engineering and Mechanics, Lehigh University, April 1990.

Visbal, M.R., "The Laminar Horseshoe Vortex System Formed at a Cylinder/Plate Juncture," AIAA paper No. 91-1826, June 1991.

VITA

The author was born in Flushing, New York in April 1966 to Thomas and Frances Fitzgerald. After graduating Flushing High School in 1984, he attended the State University of New York at Buffalo and subsequently transferred to the State University of New York at Stony Brook where he received a Bachelor of Engineering degree in Mechanical Engineering in the Spring of 1990. The author was then accepted to the graduate program at Lehigh University to concurrently work on both a Master of Science degree and a Ph.D. degree in the Mechanical Engineering Department. In October of 1993, he earned a Master of Science Degree in Mechanical Engineering. The author plans to pursue a teaching career after gaining experience in industrially related subjects of Mechanical Engineering.

END

OF

TITLE